




Cite this: *RSC Adv.*, 2021, 11, 27135

# Electrochemical sensing platform for the simultaneous femtomolar detection of amlodipine and atorvastatin drugs†

Tayyaba Kokab,<sup>a</sup> Afzal Shah,<sup>a</sup>  <sup>✉</sup> M. Abdullah Khan,<sup>\*b</sup> Jan Nisar <sup>c</sup> and Muhammad Naeem Ashiq<sup>d</sup>

The development of a proficient and ultra-high sensitive functionalized electrode for accurate analysis of drugs is a long-standing challenge. Herein, we report an electrochemical nanocomposite scaffold, comprising of silver nanoparticles integrated with functionalized carbon nanotubes (COOH-CNTs/Ag/NH<sub>2</sub>-CNTs) for the simultaneous quantification of two widely used amlodipine (AM) and atorvastatin (AT) drugs. The sandwiched nanocomposite materials were thoroughly characterized morphologically and structurally. The nanocomposite COOH-CNTs/Ag/NH<sub>2</sub>-CNTs immobilized over glassy carbon electrode catalyzed electron transfer reactions at the electrode–electrolyte interface and facilitated detection of targeted drugs, as revealed by the significant decrease in oxidation potentials at 879 mV and 1040 mV and improved current signals. Electrochemical characterization and testing show that the functionalized porous architecture with a large effective surface area is a promising scaffold for the sensing of a binary mixture of AM and AT with limits of detection in the femtomolar range (77.6 fM, and 83.2 fM, respectively). Besides, the specificity, stability, and reliability of the electrochemical sensing platform in simple and complex biological and pharmaceutical samples with high percentage recoveries highlight its scope for practical applications. Computational studies supported the experimental outcomes and offered insights about the role of modifier in facilitating electron transfer between transducer and analytes.

Received 9th June 2021  
Accepted 30th July 2021

DOI: 10.1039/d1ra04464h

rsc.li/rsc-advances

## 1. Introduction

Antihypertensive and antihyperlipidemic medications are widely used for the reduction of high blood pressure and low-density lipoprotein content in the blood stream.<sup>1</sup> For instance, amlodipine besylate (AM) is chemically a dihydropyridine derivative that antagonizes the calcium ions transmembrane influx.<sup>2</sup> It is used as a peripheral arterial vasodilator to relieve angina and hypertension. The AM kinetically interacts with the Ca<sup>2+</sup> ion receptor binding site in a gradual association and dissociation process (pK<sub>a</sub> 8.6).<sup>3</sup> This imparts a gradual onset effect, high oral bioavailability, and longer lifespan in humans than other antihypertensive drugs.<sup>4</sup> Moreover, it is used alone or in combination with other drugs of its class. Whereas the atorvastatin calcium (AT); a trihydrate calcium salt (2 : 1) acts as

a lipid-lowering agent.<sup>5</sup> The AT lowers the biosynthesis of sterols by selectively interfering with the 3-hydroxy-3-methylglutaryl-coenzyme A (HMG-CoA) reductase activity at pK<sub>a</sub> 4.5, thus, finds use in hyperlipidemia therapy.<sup>6</sup> At the same time, the combined dosage of AM and AT has been established in commercial tablets owing to their superior integrated potency for reducing cardiovascular risks.<sup>7</sup> However, their over dosages can lead to hypotension and shock and increase the risk of heart attack and kidney/liver damage. Therefore, their biological and pharmacological studies require the development of a sensitive platform for their synchronized detection in physiological fluids and pharmaceutical dosages.

The synchronized detection of multianalyte in one go is a proficient analytical strategy than a single component assay. This can save a considerable workup time for analysis, amount of analyte, and procedure cost particularly for complicated pharmaceutical dosage.<sup>7,8</sup> Literature survey reveals that the simultaneous determination of the AM and AT has been reported by employing classical techniques such as chromatography and spectroscopy.<sup>9–11</sup> These methods involve tedious workup, and multiple pre-sampling steps and selectivity issue due to the interference of excipients. In contrast, electroanalytical techniques are highly sensitive, selective, fast, and user-friendly.<sup>12,13</sup> In this quest, only two articles<sup>14,15</sup> have been reported for the electrochemical simultaneous micromolar

<sup>a</sup>Department of Chemistry, Quaid-i-Azam University, Islamabad, 45320, Pakistan. E-mail: afzals\_qau@yahoo.com

<sup>b</sup>Renewable Energy Advancement Laboratory, Department of Environmental Sciences, Quaid-i-Azam University, Islamabad, 45320, Pakistan

<sup>c</sup>National Centre of Excellence in Physical Chemistry, University of Peshawar, Peshawar 25120, Pakistan

<sup>d</sup>Institute of Chemical Sciences, Bahauddin Zakaryia University, Multan 6100, Pakistan

† Electronic supplementary information (ESI) available. See DOI: 10.1039/d1ra04464h



determination of AM and AT drugs using bare glassy carbon electrode and graphite pasted electrode respectively. Thus, electrocatalytic materials and methods are scarce on the synchronized femtomolar detection of these compounds in physiological/pharmaceutical samples. Moreover, the lack of an established redox mechanism and poor reported limits of detections<sup>2,4,6,7</sup> of AM–AT drugs suggest the development of an ultra-sensitive platform with promising features for practical applications.

The design of the experiment (DoE) of this work has been established on square-wave anodic stripping voltammetry (SWASV) owing to its preconcentration steps for analyte deposition on the electrode surface, rapid response, and operating ease which delivers remarkable analytical features for the analysis of pharmaceutical and physiological fluids samples.<sup>13,16</sup> Bare working electrodes impose high overpotentials for the redox processes which necessitates the requirement of an electrode modifier for improving the performance of electrochemical sensing platforms.<sup>2,8</sup> In this regard literature survey shows an overwhelming focus on electrocatalysts based on carbonaceous materials<sup>17,18</sup> and nanomaterials,<sup>19</sup> for the detection of the targeted drugs. For instance, carbon nanotubes (CNTs) can provide an efficient pathway to mediate charge transfer between the analyte and the electrode surface.<sup>18</sup> The functionalization of CNTs *via* organic or inorganic moieties, is significantly important to improve their dispersion, compatibility in composite/biological materials, interfacial strength, manipulation, processability, and other aspects. Specifically for the electrochemical sensors, the acidic/basic functionalization of CNTs (fCNTs) can tune the electrocatalytic activity along with physicochemical properties.<sup>20</sup> Further, their hybridization with biocompatible nanomaterials such as metal (iron, gold, zinc, copper, and silver, *etc.*) nanoparticles (M NPs) renders exceptional surface reactivity and electrochemical recognition capacity to the designed sensing platform.<sup>19,21</sup> Particularly, the exceptional conductivity, adsorption ability and electrostatic interaction ability between the layers of CNTs and M NPs on hybridization has enabled us to develop ultrahigh-sensitive electrochemical platform for AM–AT synchronized detection.

In the present work, we have designed a sandwiched nanocomposite of COOH-CNTs/Ag/NH<sub>2</sub>-CNTs by intercalation of the silver (Ag) NPs between the COOH-CNTs and NH<sub>2</sub>-CNTs layers. The fCNTs layers offer abundant acidic/basic sites to discriminate the analytes and boost up the electron-transfer process.<sup>18</sup> Furthermore, they have an affinity to stabilize and prevent the Ag NPs aggregation by electrostatic interactions.<sup>22</sup> Moreover, the sensing surface possesses electrode-anchoring hydrophobic parts and drug interacting functionalities that produce synergic effect for the interaction with the drugs and act as connecting bridge and facilitator between the transducer (host) and guest (target analytes). The devised COOH-CNTs/Ag/NH<sub>2</sub>-CNTs modified glassy carbon electrode (GCE) was then applied for the synchronized analysis of AM–AT in binary mixtures by applying the SWASV technique. This newly designed sensing probe demonstrated promising electrocatalytic activity by shifting the AM–AT oxidation peak potential to a remarkably lower value and enhancing the peak current intensity because of the

synergistic effects of its components. Moreover, we have obtained multifold high SWASV response for the target drug on COOH-CNTs/Ag/NH<sub>2</sub>-CNTs/GCE than bare GCE on our DOE, which leads to high sensitivity of the designed sensor. Because during the pre-concentration step of SWASV, the drugs functional groups with sensing surface and get reduced at its absorptivity sites. Thus, the increase of drug adsorption amount at COOH-CNTs/Ag/NH<sub>2</sub>-CNTs/GCE surface leads to significant enhancement of sensitivity. Further, at the interference studies of the bi-analyte mixture, the sensor presented favorable selectivity % RSD < 2. Likewise, the designed sensor has high viability and accuracy for the simultaneous electroanalysis of the AM–AT in real samples of tablets, tap/drinking water, sweat/saliva, and urine/serum samples. The results infer the novelty of this work based on the superior figure of merits of the nanocomposite-based sensor and its excellent stability. In addition, the synergistic role of fCNTs and Ag NPs to pre-concentrate and catalyze the AM–AT oxidation at its surface was supported by density functional theory (DFT) and hybrid meta-functional (M06-2X) computational studies. To the best of our knowledge, no previous article on the simultaneous determination of AM and AT drugs at the biocompatible COOH-CNTs/Ag/NH<sub>2</sub>-CNTs/GCE has been reported.

## 2. Experimental section

### 2.1. Chemical reagents

The pristine, acid and base functionalized CNTs (COOH-CNTs and NH<sub>2</sub>-CNTs), and Ag NPs (10 nm, containing 0.1 mM Ag in 20 mL water) were obtained from DropSens. While, all other analytical grade chemicals were procured from Alfa Aesar, Merck Germany, and/or Sigma Aldrich. The amlodipine besylate (AM) and atorvastatin calcium (AT) drugs were used to prepare analytes solutions in methanol and ethanol, respectively. Likewise, amino acids (alanine, cysteine, glutamic acid, glycine, lysine, leucine, threonine), metal salts (arsenic chloride, ammonium chloride, aluminium chloride, barium nitrate, chromium nitrate, caesium chloride, calcium bicarbonate, copper sulphate, cadmium nitrate, cobalt chloride, ferric chloride, lead nitrate, manganese chloride, magnesium stearate, mercury chloride, nickel sulphate, potassium phosphate, silver nitrate, strontium nitrate, sodium carbonate, thallium sulphate, titanium oxide, zinc acetate), organic acids (ascorbic acid, citric acid, folic acid, oxalic acid, succinic acid, salicylic acid, tannic acid, uric acid, usnic acid), disaccharides (fructose, glucose, galactose, lactose, maltose, sucrose), organic compounds (dopamine, EDTA, ethanol, glycerol, riboflavin, thymidine, urea, 2-amino-4-nitrophenol, 4-aminophenol, 3-chloro-5-nitrophenol), and surfactants (CTAB, SDS) were used for the preparation of solutions which were employed for the investigating the influence of organic/inorganic interfering agents. The acetate buffer solution (ABS), Britton Robert buffers (BRB), and phosphate buffer solution (PBS), HCl, H<sub>2</sub>SO<sub>4</sub>, H<sub>3</sub>BO<sub>3</sub>, H<sub>3</sub>PO<sub>4</sub>, KCl, and NaOH were used to prepare stripping electrolytes. The glassware was washed with conc. HNO<sub>3</sub> and doubly deionized water (ddw) before use.



## 2.2. Development of COOH-CNTs/Ag/NH<sub>2</sub>-CNTs working electrode

The GCE surface possesses multiple units of alcohols, aldehydes, carboxylic acids, ketones, lactones, and quinones on its sp<sup>2</sup> hybridized carbon conjugated rings system.<sup>23</sup> Before fabrication, the physiochemical cleaning steps upgrade the O/C ratio of the GCE surface. Thus, the GCE surface was rubbed on a nylon cushion with  $\mu$ -Al<sub>2</sub>O<sub>3</sub> slurry, gently until a shiny and smooth surface was attained. Consequently, it was rinsed with ddw, ethanol, and aq. HNO<sub>3</sub> (1 : 1, v/v) and then, dried at room temperature with air. Afterward, the GCE was chemically cleaned by multiple reversible cyclic voltammetric (CV) cycles at potential −0.2 V to +1.8 V in 0.1 M HClO<sub>4</sub> until a reproducible surface was attained.

The COOH-CNTs, and NH<sub>2</sub>-CNTs were dispersed in 1 mg/1 mL dimethyl formamide (DMF) by conducting a 2 hour ultrasonication before use. The activated GCEs were modified by drop-casting of NH<sub>2</sub>-CNTs, COOH-CNTs, and Ag NPs dispersions through mixed and layer-by-layer (LBL) methods.<sup>22</sup> For the mixed method, the 50  $\mu$ L of each, Ag NPs, COOH-CNTs, and NH<sub>2</sub>-CNTs dispersion were mixed by ultra-sonication for 1 hour. Then, the COOH-CNTs–NH<sub>2</sub>-CNTs–Ag/GCE was fabricated by employing 5  $\mu$ L of this mixture on pre-activated GCE and dried at 50 °C in a vacuum oven. In the LBL fabrication process, the 5  $\mu$ L of COOH-CNTs was deposited on the pre-cleaned GCE surface. Then, 2  $\mu$ L drop of Ag NPs was carefully coated on the devised COOH-CNTs/GCE. After that, the modified electrode represented as COOH-CNTs/Ag/NH<sub>2</sub>-CNTs/GCE was developed by employing a 5  $\mu$ L drop of NH<sub>2</sub>-CNTs (1 mg mL<sup>−1</sup>) on the assembled Ag/NH<sub>2</sub>-CNTs/GCE (Scheme 1). To attain an even and properly adsorbed modifier layer on the GCE surface, after each coating the recognition layer was dried at 50 °C in a vacuum oven. For comparative analysis, CNTs/GCE, Ag NPs/GCE, NH<sub>2</sub>-CNTs/GCE, COOH-CNTs/GCE, g-C<sub>3</sub>N<sub>4</sub>/GCE, Au NPs/GCE, ZnO NPs/GCE, Au–Ag (1 : 1) NPs/GCE, Au–Ag (1 : 2) NPs/GCE, Au–Cu (1 : 1) NPs/GCE, Au–Cu (1 : 2) NPs/GCE, Au–Cu (1 : 3) NPs/GCE, Au–Cu (2 : 1) NPs/GCE, Au–Cu (3 : 1) NPs/GCE, Ag–Cu (1 : 1) NPs/GCE, Au–g-C<sub>3</sub>N<sub>4</sub>/GCE, Ag–g-C<sub>3</sub>N<sub>4</sub>/GCE, Sn–g-C<sub>3</sub>N<sub>4</sub>/GCE, Fe–g-C<sub>3</sub>N<sub>4</sub>/GCE, Co–g-C<sub>3</sub>N<sub>4</sub>/GCE, Zn–g-C<sub>3</sub>N<sub>4</sub>/GCE, Mo–g-C<sub>3</sub>N<sub>4</sub>/GCE, Ni–g-C<sub>3</sub>N<sub>4</sub>/GCE, and CNTs/Ag–g-C<sub>3</sub>N<sub>4</sub>/GCE, were also developed one by one *via* casting 5  $\mu$ L amount of each of the commercial and/or synthesized modifier. Moreover, all dried prepared working electrodes were cautiously rinsed with ddw and PBS solution to strip off slackly bound modifying material prior to electrochemical use. After each electrochemical measurement, the modified electrode was cleaned by 5 scans of CV cycles run in PBS of pH 6 from 0 V to 1.0 V, to remove the deposited analytes. Conversely, no significant decay was observed in the performance of the designed electrode which confirmed firm interaction of nanocomposite with the chemical functionalities of the activated GCE surface.<sup>24</sup>

## 2.3. Characterization of the modified electrode and design of experiment

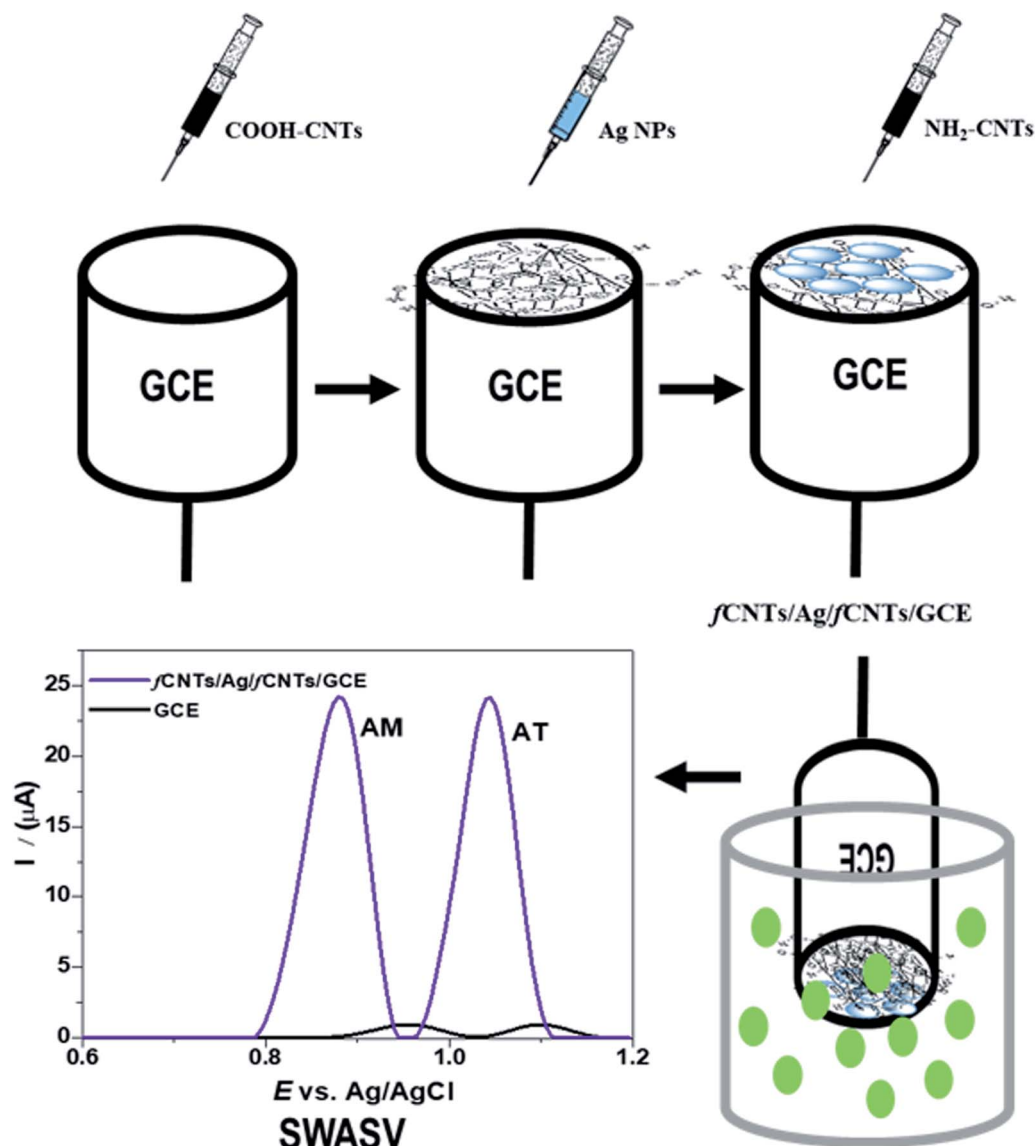
An X-ray diffractometer (Panalytical 3040/60 X pert PRO diffractometer) with CuK $\alpha$  as an X-rays source at 40 kV voltage

and 40 mA current was used to determine the structural properties of nanomaterials modifiers. The scan was run at an angle 2 $\theta$  from 10° to 70° at a scan rate of 0.01° s<sup>−1</sup>. Likewise, the UV-visible (Shimadzu 1601) spectrophotometer, having quartz cuvettes of 1 cm path length and wavelength range from 200–1100 nm, was operated to study the optical features of the nanomaterials-based modifiers. Further structural characterization of the designed sensor was performed on Thermo Scientific Nicolet 6700 Fourier transform infrared spectrometer (FTIR) U.S, in the wavelength range from 400–4000 cm<sup>−1</sup>. The data obtained from these techniques were employed to study the crystallographic configuration, optical behavior, and introduced functionalities of the as-synthesized products, Ag NPs, COOH-CNTs, NH<sub>2</sub>-CNTs, and COOH-CNTs/Ag/NH<sub>2</sub>-CNTs. Likewise, for chemical compositions, and morphological characterization, the scanning electron microscope (SEM) investigation along with energy-dispersive X-ray spectroscopy (EDX) were performed on ZEISS EVO 40 (Merlin, Carl Zeiss). Furthermore, the electrochemical impedance spectroscopy (EIS) and cyclic voltammetry (CV) were operated for electrochemical characterization of the modified GCE. Moreover, the design of experiment (DOE) based on the square wave anodic stripping voltammetry (SWASV) method was established for the analyte's detection. All electrochemical measurements were executed at Metrohm Auto lab PGSTAT 302N Switzerland (Fig. S1a†) by NOVA 1.1 software on PC controlled system. A standard electrochemical cell consisted of a 3-electrode system as shown in Fig. S1b,† where the working electrode (WE) was a glassy carbon electrode (GCE) of 0.071 cm<sup>2</sup> surface area or the designed modified electrode, reference electrode (RE) was Ag/AgCl (conc. KCl), and platinum wire was used as an auxiliary electrode (AE). To prevent inconsistency in voltammograms all the measurements were conducted in N<sub>2</sub> atmosphere at ambient temperature (23–27 °C). In addition, a digital INOLAB pH meter, Xylem Analytics Germany was used for buffer and working solutions pH controls. An ultrasonic model ELMASONIC S10H was used for nanomaterials dispersion, electrode cleaning, and apparatus washing.

## 2.4. Electrochemical measurements

The 1 mM AM and AT stock solutions were prepared in 100 mL volumetric flask with methanol and ethanol solvents, respectively. Then, the solution flasks were wrapped with aluminum foil to shield them from light and kept in a dark place. For AM and AT working solutions, the stock solutions were diluted with a constant 20/80 (v/v) ratio of their respective solvents and PBS (pH 6) to avoid any solubility problems. The designed electrode COOH-CNTs/Ag/NH<sub>2</sub>-CNTs/GCE was placed in an electrochemical cell for the sensing of AM (6  $\mu$ M) and AT (9  $\mu$ M) mixture in PBS of pH 6 by SWASV method. At 0 V deposition potential, the analytes get accumulated onto the sensing surface under stirring of solution for 125 s (deposition time). Afterward, an equilibrium time of 5 s was retained in quiescent solution, and then the SWASV scan was run from a potential of 0.6 V to 1.2 V at 20 Hz frequency, by an increment of 0.5 mV potential, 100 mV s<sup>−1</sup> scan rate and 20 mV pulse amplitude.





Scheme 1 The fabrication and application of COOH-CNTs/Ag/NH<sub>2</sub>-CNTs nanocomposite sensor.

### 2.5. Preparation of pharmaceutical and biological samples

To check the reliability of the designed electrode COOH-CNTs/Ag/NH<sub>2</sub>-CNTs/GCE for AM and AT drugs, multiple complex matrixes of commercial tablets, tap & drinking water, human blood, urine, and artificial sweat/saliva samples were used. For commercial dosage, ten tablets of each type (AM, AT, and AM-AT) were precisely weighed and ground in a mortar by a pestle. Then, an equivalent weight of the powder corresponding to 1 mM stock solution of its actives was completely dissolved in respective solvents by sonication. Then, the clear supernatant liquor designated as the stock solution was obtained after filtration of suspension. It was covered with aluminum foil and kept in a dark. Afterward, for SWASV measurement the working solutions were prepared by the successive dilutions of the tablets stock solutions with 20/80 (v/v) ratio of solvent and PBS (pH 6). The initial contents of the AM and AT in their pharmaceutical dosages were calculated referring to the

corresponding regression equations of their calibration plots. Moreover, to investigate the potential effect of the tablet excipients, the precise quantities of AM and AT actives were assessed by a standard addition recovery method. For this purpose, the known amounts of AM and AT from freshly prepared standard solutions were spiked in pre-analyzed tablet solutions and each measurement was triplicated to calculate accurate recovery percentages.

Likewise, the standard solutions of urine and blood were prepared after collection from healthy volunteers. To remove protein scums from urine/blood samples, the 5.4 mL acetonitrile, 3.6 mL urine/serum, and 1 mL of solvent/drug (from 1 mM stock solution) were centrifuged in a 15 mL tube for 25 min at 5k rpm. The supernatant liquors were designated as stock solutions of urine/serum, collected by filtration through 0.22 μm pore size membrane. Again, the stock solutions were diluted by 20/80 (v/v) ratio of solvent and PBS (pH 6) ratio to attain





analyzable solutions. The urine/serum sample when not in use were stored in the refrigerator at 4 °C. Moreover, the synthetic saliva samples were prepared by dissolving 0.25 g NaCl, 2.1 g NaHCO<sub>3</sub>, 15 mg NaNO<sub>3</sub>, and 0.1 g K<sub>2</sub>CO<sub>3</sub> in 0.5 L ddw of pH 5 adjusted by dil. NaOH or HNO<sub>3</sub> drops. Likewise, the artificial sweat samples were prepared by adding 1 mM KCl, 1 mM lactic acid, 7.5 mM NaCl, and 1 mM urea in PBS solutions.<sup>25</sup> Both sweat and saliva samples were used immediately after preparation. The urine/serum/saliva/sweat samples were SWAVS analyzed under optimized conditions for initial content assessment (if any). Afterward, the percentage recovery experiments of the above-mentioned drugs in the real sample matrixes were executed by standard spiking method to authenticate the precision and anti-interferent ability of the proposed methodology.

## 2.6. Theoretical calculations

To associate the theoretical findings with voltammetric data, the intermolecular interactions of the AM and AT with Ag NPs decorated fCNTs matrix, that controls the enhancement of the electrochemical signal, was probed by the DFT and M06-2X measurements at Gaussian 09 (G09) software package. Firstly, the AM and AT molecular geometries were optimized by DFT (B3LYP) method with 6-311G++(d,p) basis set. Their chemical descriptors such as HOMO, LUMO, bandgap ( $E_g$ ) [ $E_{\text{LUMO}} - E_{\text{HOMO}}$ ], ionization potential IE ( $-E_{\text{HOMO}}$ ), electron affinity EA ( $-E_{\text{LUMO}}$ ), global hardness  $\eta$  [ $(\text{IE} - \text{EA})/2$ ], electronegativity  $\chi$  [ $(\text{IE} + \text{EA})/2$ ], chemical softness  $\sigma$  ( $1/\eta$ ), electronic chemical potential  $\mu$  ( $-\chi$ ), and electrophilicity  $\Omega$  ( $\mu^2/2\eta$ ) were calculated in their respective solvents.<sup>26</sup> Furthermore, the catalytic mechanism of the sensor due to noncovalent interactions of Ag NPs and fCNTs toward AM and AT drugs were computationally assessed by M06-2X functional. For this purpose, Ag NPs were marked as a triangle Ag<sub>3</sub> system,<sup>27</sup> while the single unit of armchair (5, 5) with four COOH groups and a single unit of armchair (5, 5) with four CONH<sub>2</sub> groups were donated as COOH-CNTs and NH<sub>2</sub>-CNTs. Then, the Ag NPs, Ag NPs/COOH-CNTs, COOH-CNTs/Ag/NH<sub>2</sub>-CNTs, and their merged structures with AM and AT were optimized at M06-2X functional with LANL2DZ basis set and their quantum descriptors were calculated to evaluate the chemical reactivity of AM and AT on the modifier surface. To consider probable  $\pi$ - $\pi$  stacking interactions, the parallel configuration of the AM and AT molecules with Ag NPs/COOH-CNTs and COOH-CNTs/Ag/NH<sub>2</sub>-CNTs were computed. Moreover, for indirect accounts of dispersion interactions and solvent effects in chemical systems, the M06-2X functional and polarized continuum model (PCM) was applied. The adsorption energies  $\Delta E$  (eV) were calculated from the theoretical data by the following equations;

$$\Delta E = E_{(\text{Ag NPs drug})} - (E_{\text{Ag NPs}} + E_{\text{drug}})$$

$$\Delta E = E_{(\text{COOH-CNTs-Ag NPs-drug})} - (E_{\text{COOH-CNTs}} + E_{\text{Ag NPs}} + E_{\text{drug}})$$

$$\Delta E = E_{(\text{fCNTs-Ag NPs-fCNTs-drug})} - (E_{\text{COOH-CNTs}} + E_{\text{Ag NPs}} + E_{\text{NH}_2\text{-CNTs}} + E_{\text{drug}})$$

whereas,  $E_{(\text{Ag NPs drug})}$ ,  $E_{(\text{COOH-CNTs-Ag NPs-drug})}$  and  $E_{(\text{fCNTs-Ag NPs-fCNTs-drug})}$  are the total adsorption energies of the drug/modifier merged structures while,  $E_{\text{COOH-CNTs}}$ ,  $E_{\text{Ag NPs}}$ ,  $E_{\text{NH}_2\text{-CNTs}}$ ,  $E_{\text{Ag NPs}}$ , and  $E_{\text{drug}}$  are the individual structure energies.<sup>28</sup>

## 2.7. Live subject statement

This study was performed in compliance with the laws of Quaid-i-Azam University bioethical committee for health care. It was approved by the ethical committee of Quaid-i-Azam University. Informed consent was obtained from the human subjects prior to obtaining urine and saliva.

# 3. Results and discussion

To find the best oxidation response of AM and AT binary mixture, different NPs and their ratios such as CNTs, COOH-CNTs, NH<sub>2</sub>-CNTs, g-C<sub>3</sub>N<sub>4</sub>, Ag NPs, Au NPs, ZnO NPs, Au-Ag (1 : 1) NPs, Au-Ag (2 : 1) NPs, Au-Ag (1 : 2) NPs, Au-Cu (1 : 1) NPs, Au-Cu (1 : 2) NPs, Au-Cu (1 : 3) NPs, Au-Cu (2 : 1) NPs, Au-Cu (3 : 1) NPs, Ag-Cu (1 : 1) NPs, Au-g-C<sub>3</sub>N<sub>4</sub> NPs, Ag-g-C<sub>3</sub>N<sub>4</sub> NPs, Sn-g-C<sub>3</sub>N<sub>4</sub> NPs, Fe-g-C<sub>3</sub>N<sub>4</sub> NPs, Co-g-C<sub>3</sub>N<sub>4</sub> NPs, Zn-g-C<sub>3</sub>N<sub>4</sub> NPs, Mo-g-C<sub>3</sub>N<sub>4</sub> NPs, Ni-g-C<sub>3</sub>N<sub>4</sub> NPs, and CNTs/Ag-g-C<sub>3</sub>N<sub>4</sub> and their combinations were deposited on GCE but COOH-CNTs/Ag/NH<sub>2</sub>-CNTs/GCE gave the best response and thus it was designated as the most suitable sensing platform in this work. The details of characterization and electrochemical performance of the designed modified electrode for AM-AT binary mixture analysis are described in the following sections.

## 3.1. Morphological and structural characterization of the designed sensor

To establish integration of Ag (NPs) with fCNTs in the fabricated NH<sub>2</sub>-CNTs/Ag/COOH-CNTs nanocomposite, their morphological and structural characterizations employing SEM, EDX, XRD, UV-vis spectroscopy, and FTIR were carried out. The XRD patterns of the COOH-CNTs/Ag/NH<sub>2</sub>-CNTs revealed face-centered cubic (FCC) Ag NPs at fCNTs matrix (Fig. 1a). Where all representative diffraction planes at 25.6°, and 39°, 45° and 64°, for CNTs, and Ag NPs, respectively are seen (JCPDS # 01-075-1621 and 00-004-0783).<sup>29</sup> Moreover, the narrow XRD diffraction peaks indicate improved crystallinity of the nanocomposite on the successful integration of the Ag NPs with the fCNTs layers. Likewise, in the optical spectrum of COOH-CNTs/Ag/NH<sub>2</sub>-CNTs characteristic red-shifted absorption peak at 426 nm relative to the Ag NPs, and distortion at lower wavelength is present (Fig. S2†).<sup>30</sup> The FTIR spectra of NH<sub>2</sub>-CNTs/Ag/COOH-CNTs, show intense absorption peaks of N-H/O-H merged band (3300–3400 cm<sup>-1</sup>), N-H (1565 cm<sup>-1</sup>, 1437 cm<sup>-1</sup>), C=O (1760 cm<sup>-1</sup>, 1675 cm<sup>-1</sup>), methylene (C-H) (2940 cm<sup>-1</sup>, 2870 cm<sup>-1</sup>, 1254 cm<sup>-1</sup>), NH<sub>2</sub> (1316 cm<sup>-1</sup>, 951 cm<sup>-1</sup>), C-O-C (1093 cm<sup>-1</sup>), C-N (901 cm<sup>-1</sup>), O=C=O (659 cm<sup>-1</sup>), and Ag-O (~625 cm<sup>-1</sup>) indicative of the coordination bonding of Ag NPs with O-H and/or C=O functionalities of integrated fCNTs in nanocomposite (Fig. 1b).<sup>31,32</sup> Additionally, the SEM micrographs of the individual and integrated structure are presented in Fig. 1c–f. The physiochemically activated GCE revealed



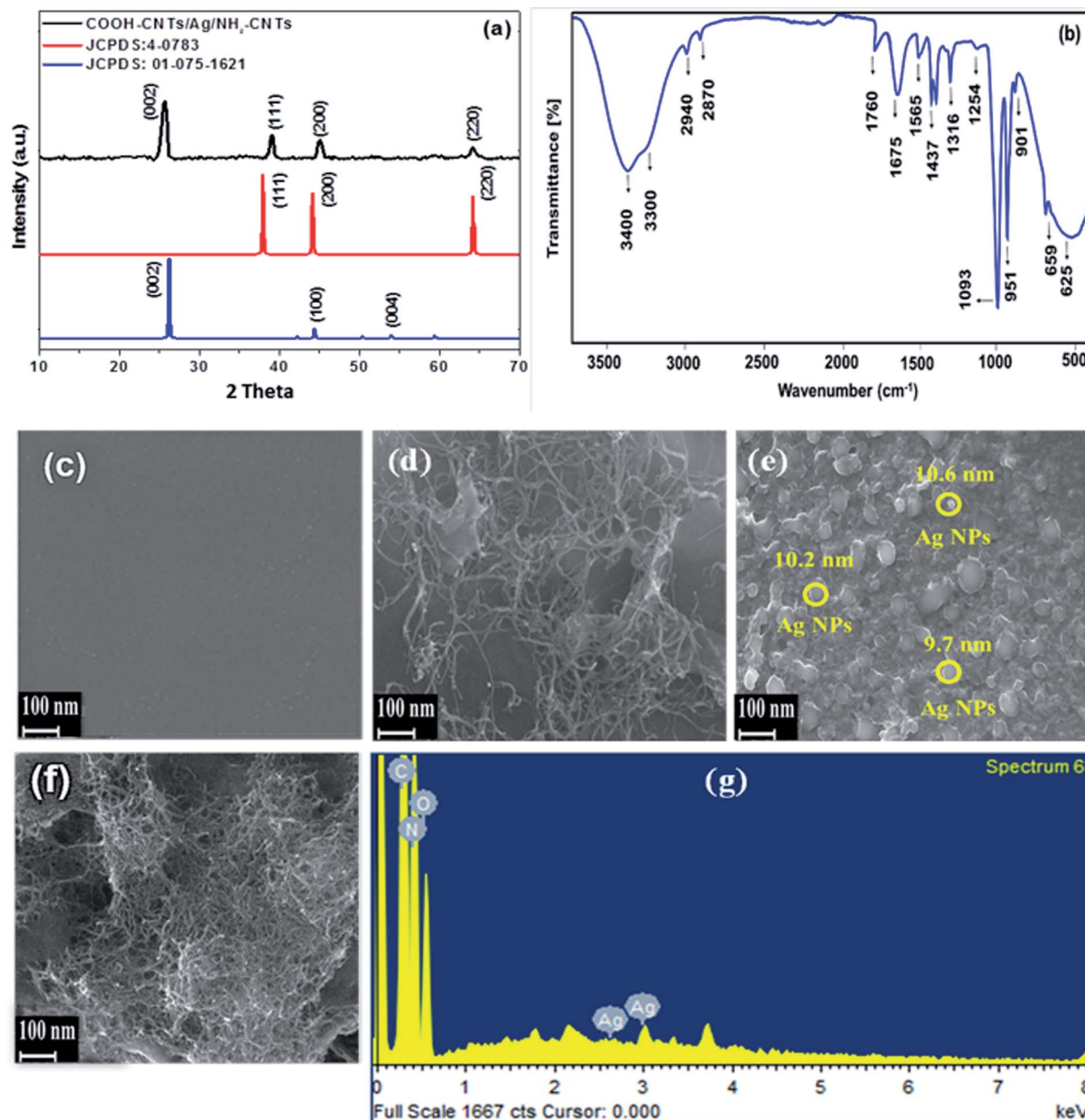


**Fig. 1** Structural characterization (a) XRD pattern of COOH-CNTs/Ag/NH<sub>2</sub>-CNTs along with JCPDS 4-0783 & 01-075-1621 which are standard XRD spectra of Ag NPs and CNTs. (b) FT-IR analysis of COOH-CNTs/Ag/NH<sub>2</sub>-CNTs. The morphological characterization, the SEM images of (c) bare GCE, (d) fCNTs fabricated GCE (e) Ag/NH<sub>2</sub>-CNTs/GCE (f) COOH-CNTs/Ag/NH<sub>2</sub>-CNTs/GCE (g) EDX spectrum of COOH-CNTs/Ag/NH<sub>2</sub>-CNTs nanocomposite film immobilized GCE.

a smooth surface (Fig. 1c), while COOH-CNTs/GCE disclosed the CNTs casted threads (Fig. 1d) where the addition of Ag NPs indicates their homogeneous dispersion at the fCNTs (Fig. 1e). The complete configuration of COOH-CNTs/Ag/NH<sub>2</sub>-CNTs/GCE presents a pronounced porous microstructure essential for accumulation and discrimination of analytes (Fig. 1f). In addition, the EDX spectrum confirmed the nanocomposite chemical composition (Ag, N, C, and O) (Fig. 1g). All these characterizations collectively supported the successful development of the sandwiched nanosensor structure held together by adjacent fCNTs electrostatic,  $\pi$ - $\pi$  and van der Waals interactions.

### 3.2. Electrochemical characterization of the designed electrode

To elucidate the fundamental understanding about charge transfer mechanism, effective surface area, the success of immobilization, and impedance changes at the sensor/analyte interfacial surfaces, the CV and EIS were executed. The modified electrode surface area plays the main role in the electrochemical analytical features of the sensor. The size to sensor properties, matters in the sensing behavior of the prepared material in terms of "active surface area". To evaluate the active surface area of the nanomaterials deposited at GCE, CV experiments were performed in 5 mM standard [Fe(CN)]<sup>3-/4</sup> redox



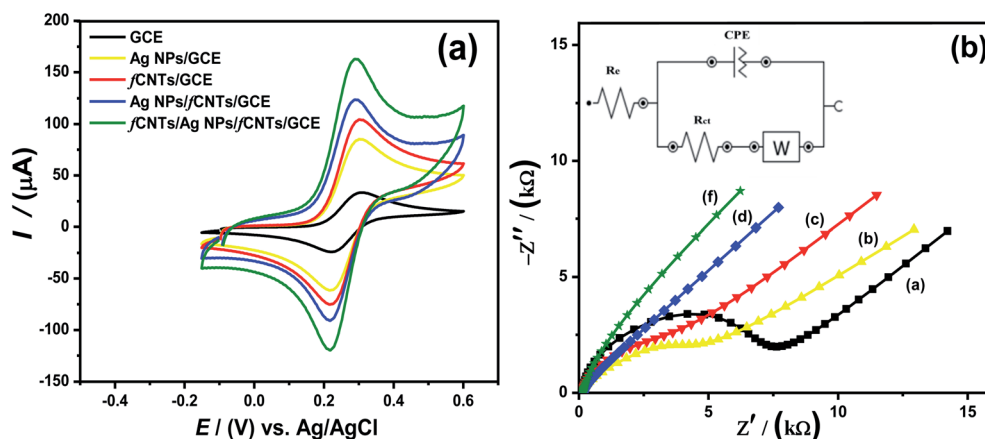


Fig. 2 (a) Cyclic voltammograms of 5 mM  $K_3[Fe(CN)_6]$  with 0.1 M KCl electrolyte at bare GCE, Ag NPs/GCE, fCNTs/GCE, Ag/NH<sub>2</sub>-CNTs/GCE, and COOH-CNTs/Ag/NH<sub>2</sub>-CNTs/GCE at scan rate 100 mV s<sup>-1</sup> from potential -1.0 V to 1.0 V (b) Nyquist plots of bare GCE, Ag NPs/GCE, fCNTs/GCE, Ag/NH<sub>2</sub>-CNTs/GCE and COOH-CNTs/Ag/NH<sub>2</sub>-CNTs/GCE using experimental EIS data at frequency scan from 0.1 Hz to 100 kHz with 10 mV amplitude in same redox probe.

Table 1 Randles equivalent circuit model fitting the EIS parameters, and CV: calculated data for bare and the fabricated GC electrodes

EIS/CV parameters	Units	Bare GCE	Ag NPs/GCE	fCNTs/GCE	Ag/fCNTs/GCE	COOH-CNTs/Ag/NH <sub>2</sub> -CNTs/GCE
$R_{ct}$	( $\Omega$ )	6379	3217	$1.25 \times 10^{-4}$	$5.25 \times 10^{-5}$	$2.0 \times 10^{-5}$
Re ( $\Omega$ )	( $\Omega$ )	159.0	156.1	162.05	160.44	131.9
CPE	( $\mu F$ )	0.45	0.73	2.39	5.91	23.5
$n$	—	0.71	0.85	0.89	0.91	0.97
A	(cm <sup>2</sup> )	0.02	0.07	0.08	0.10	0.14

probe at 100 mV s<sup>-1</sup> scan rate. The working surface area of the electrodes calculated by Randles-Sevcik equation<sup>2</sup>, were 0.02 cm<sup>2</sup> (bare GCE), 0.07 cm<sup>2</sup> (Ag NPs/GCE), 0.10 cm<sup>2</sup> (Ag/NH<sub>2</sub>-CNTs/GCE) and 0.14 cm<sup>2</sup> (COOH-CNTs/Ag/NH<sub>2</sub>-CNTs/GCE) respectively, exhibit a sevenfold increase for nanocomposite compared to bare GCE electrode (Fig. 2a, Table 1). Moreover, at nanocomposite sensing platform the maximum peak current signals and lowest peak potential difference; evidence of its boosted electrocatalytic activity than unmodified GCE and other modified electrodes. Likewise, the EIS spectra of bare GCE, Ag NPs/GCE, Ag/NH<sub>2</sub>-CNTs/GCE and COOH-CNTs/Ag/NH<sub>2</sub>-CNTs/GCE was fitted with Randle's equivalent circuit model shown in Fig. 2b, while parameters attained from Nyquist plots are summarized in Table 1.<sup>33</sup> The bare GCE possesses higher  $R_{ct}$  value of 6379  $\Omega$  revealing passive electrochemical diffusion process. While the COOH-CNTs/Ag/NH<sub>2</sub>-CNTs/GCE's significant low value of  $R_{ct}$  elucidates promising charge transfer kinetics with improved conductivity of the redox probe than other electrodes tested in this work. Furthermore, the EIS results validate the successful immobilization of COOH-CNTs/Ag/NH<sub>2</sub>-CNTs recognition layer with a uniform surface (CPE value) and utmost capacitor character ( $n$  value).

### 3.3. Voltammetric analysis of the target drugs at the designed sensing surface

To test the electrochemical response of target drugs, CV and SWASV perform in AM (6  $\mu M$ ) and AT (9  $\mu M$ ) mixture at bare GCE and modified electrodes. At bare GCE, the weak AM and AT irreversible oxidation reaction peaks were observed at oxidation potential of 911 mV and 992 mV, respectively due to unstable oxidized products.<sup>2</sup> On the contrary, the well-resolved voltammograms were noticed at all the modified GCEs particularly, at COOH-CNTs/Ag/NH<sub>2</sub>-CNTs/GCE (Fig. 3a). The oxidation potentials of AM and AT appeared at 821 mV and 970 mV, respectively which revealed significant negative potential shift.<sup>2,6</sup> In addition, the SW voltammograms of AM and AT reveal weak signals at bare GCE whereas, well defined and amplified peaks appeared for all other tested nanosensors (Fig. 3b). Notably, COOH-CNTs/Ag/NH<sub>2</sub>-CNTs modified GCE exhibited superior capability to accumulate the drug molecules *via* host-guest complex formation. The multi-fold magnified anodic peak current of AM and AT at the COOH-CNTs/Ag/NH<sub>2</sub>-CNTs/GCE was spotted with a significant shift towards low overpotential from 954 mV to 1100 mV for AM and 835 mV to 1040 mV for AT compare to the bare GCE. These outcomes of SWASV, EIS and CV elucidate the outstanding electrocatalytic activity, facile



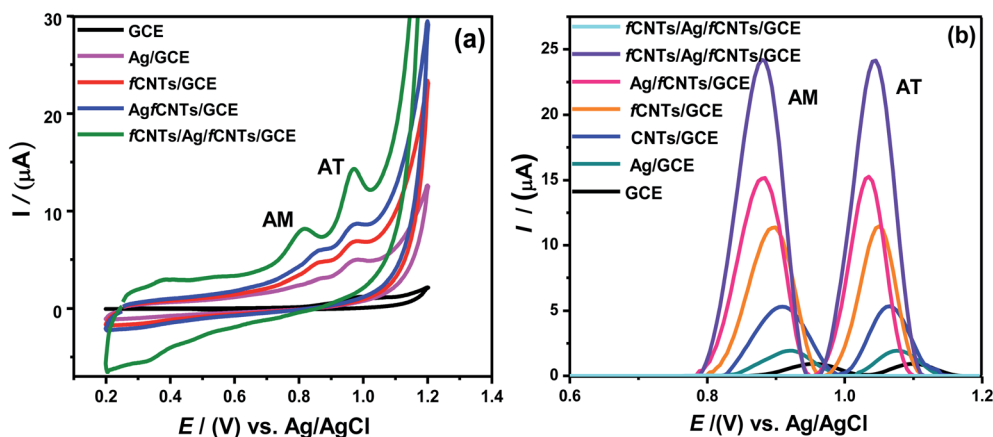


Fig. 3 (a) Cyclic voltammograms of AM (6 μM) and AT (9 μM) mixture at bare GCE, Ag NPs/GCE, fCNTs/GCE, Ag/NH<sub>2</sub>-CNTs/GCE and COOH-CNTs/Ag/NH<sub>2</sub>-CNTs/GCE, in PBS of pH = 6, at 100 mV s<sup>-1</sup> scan rate from potential 0.2 V to 1.2 V. (b) The SWASV obtained from potential 0.6 V to 1.2 V at bare GCE, Ag NPs/GCE, CNTs/GCE, COOH-CNTs/GCE, COOH-CNTs/GCE, Ag/NH<sub>2</sub>-CNTs/GCE, and COOH-CNTs/Ag/NH<sub>2</sub>-CNTs/GCE for the detection of AM (6 μM) and AT (9 μM) mixture in pH 6 PBS, at 100 mV s<sup>-1</sup> scan rate, 0 V deposition potential and accumulation time of 125 s. The SWASV blank run in 1 : 1 of aqueous solvent and PBS (pH 6) stripping solvent at COOH-CNTs/Ag/NH<sub>2</sub>-CNTs/GCE under same experimental conditions.

interfacial transduction and effective sensing ability of the modified electrode due to the synergy among the noble metal NPs and fCNTs layers in the sandwiched matrix. Therefore, the COOH-CNTs/Ag/NH<sub>2</sub>-CNTs/GCE was chosen for synchronized detection of the AM and AT through the SWASV.

### 3.4. Influence of experimental parameters

The voltammetric parameters such as the nanomaterials amount, preconcentrating potential, and deposition time, control the sensitivity and intensity of the signals of AM-AT drugs, at COOH-CNTs/Ag/NH<sub>2</sub>-CNTs/GCE (Fig. S3–6†).

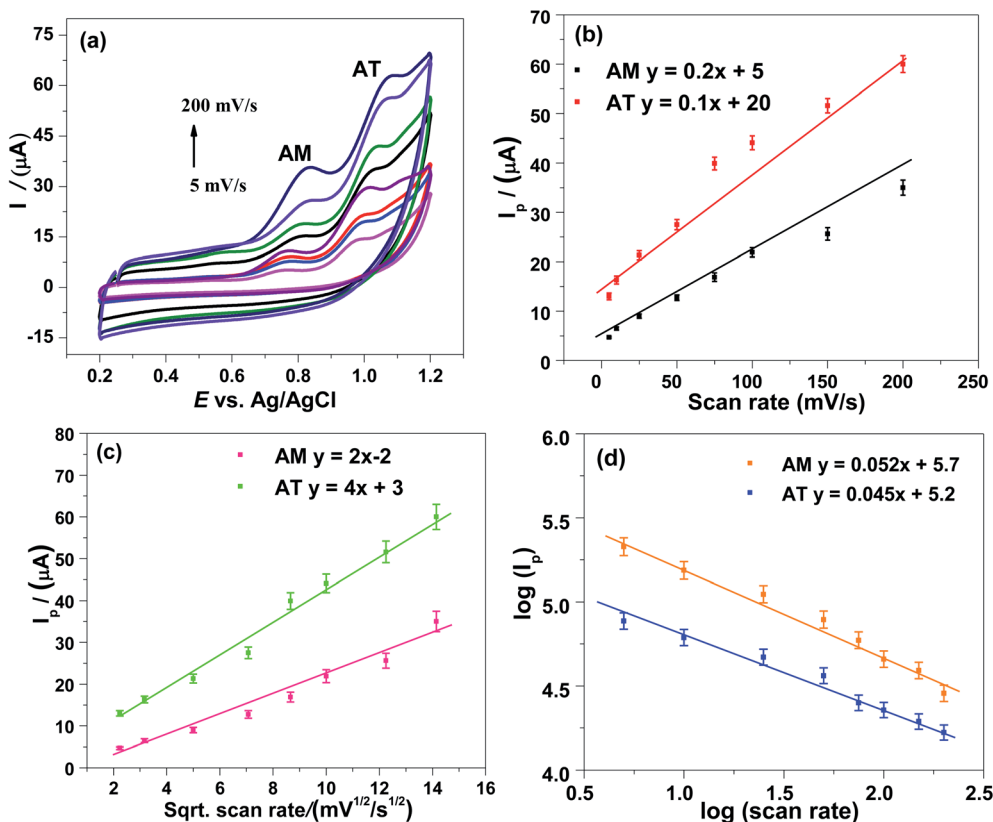


Fig. 4 (a) Cyclic voltammograms of AM (0.1 mM) and AT (0.1 mM) mixture at COOH-CNTs/Ag/NH<sub>2</sub>-CNTs/GCE in PBS of pH 6 by varying scan rate from 5 mV s<sup>-1</sup> to 200 mV s<sup>-1</sup> at potential 0.2 V to 1.2 V (b) plot of the peak currents of AM and AT vs. scan rate (mV s<sup>-1</sup>) (c) the AM and AT peak currents plot vs. square root of (scan rate) (d) plot of log of AM and AT peak currents vs. log(scan rate).

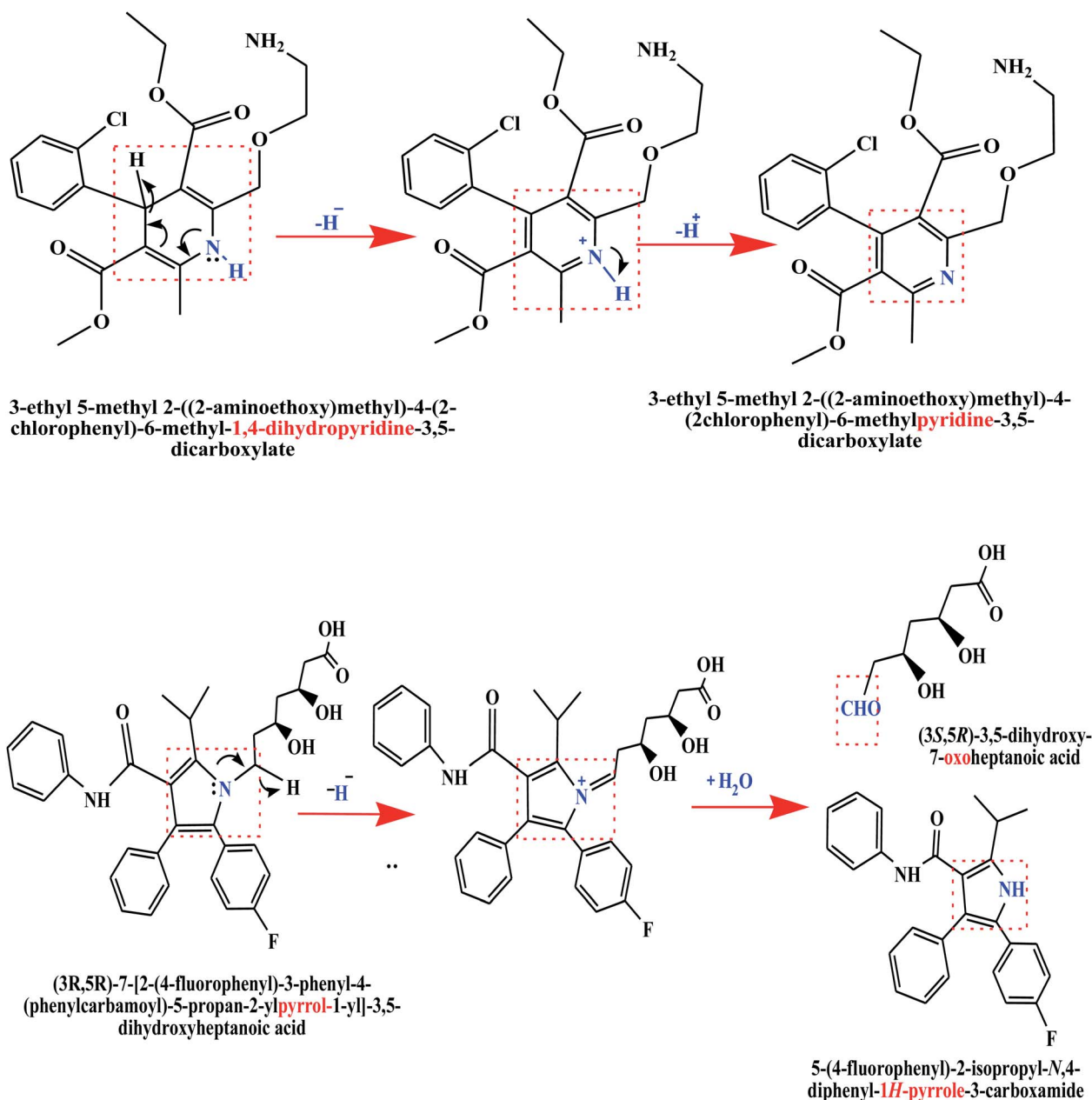




Additionally, the electrochemical oxidation mechanism of the AM-AT and electrocatalyst sensing pathway at COOH-CNTs/Ag/NH<sub>2</sub>-CNTs nanocomposite devised sensor was studied by the scan rate and supporting electrolyte pH variation.

**3.4.1. Effects of scan rate.** The scan rate ( $\nu$ ) variation relationship with the peak potentials ( $E_p$ ) and peak currents ( $I_p$ ) of AM and AT cyclic voltammograms was probed at scan rate 5 mV s<sup>-1</sup> to 200 mV s<sup>-1</sup>, as illustrated in Fig. 4a. The CV profiles displayed the gradual increase of redox signals of both drugs on the increment of the scan rate ( $\nu$ ). The scan rate variation data suggest the diffusion and/or adsorption-controlled redox process at the sensor surface. The analysis of established  $I_p$  vs.  $\nu$  and  $I_p$  vs.  $\nu^{1/2}$  plots infers a diffusion-control process at the

designed sensor (Fig. 4b and c). Likewise, the  $\log I_{pa}$  vs.  $\log \nu$  slopes of AM and AT were closest to an ideal reaction of solution species (Fig. 4d). Which further support the occurrence of a diffusion-controlled process for the AM-AT oxidation at COOH-CNTs/Ag/NH<sub>2</sub>-CNTs/GCE. Additionally, the AM-AT anodic peak potentials ( $E_{pa}$ ) were shifted positively on the potential scan rate increment, which is a representative feature of an irreversible oxidation process. Akin to this, the AM and AT anodic peaks with no associated cathodic peaks in the reverse scan, indicate their irreversible oxidation at COOH-CNTs/Ag/NH<sub>2</sub>-CNTs/GCE. Moreover, according to the Laviron equation, the linear relation of  $E_p$  vs.  $\log \nu$  plots further validates the irreversibility of the AM-AT electrochemical oxidation process



Scheme 2 Proposed electrochemical oxidation mechanisms of AM and AT.



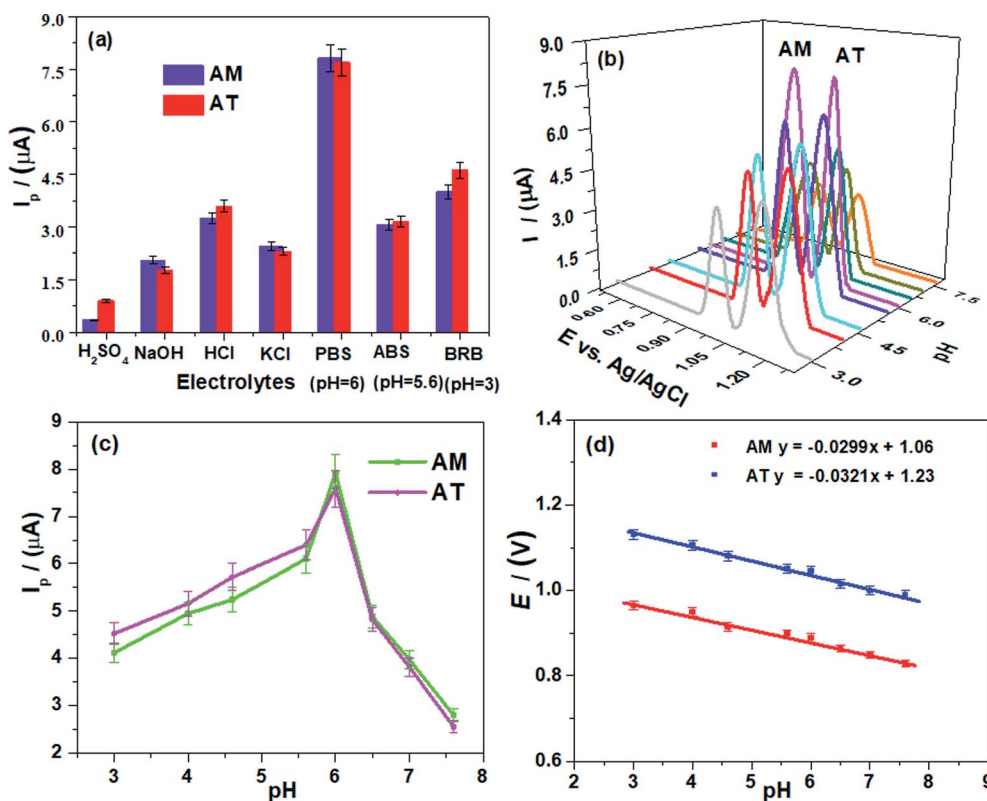


Fig. 5 (a) Bar graph of 0.1 M  $H_2SO_4$ , 0.1 M NaOH, 0.1 M HCl, 0.1 M KCl, PBS (pH 6), ABS (pH 5.6), and BRB (pH 3) supporting media effect on the SWASV current peaks values of AM (6  $\mu M$ ) and AT (9  $\mu M$ ) mixture at 0 V deposition potential and 5 s deposition time through LBL modification of GCE with COOH-CNTs/Ag/NH<sub>2</sub>-CNTs/GCE at 100  $mV s^{-1}$  scan rate. (b) The SWASV graphs as a function of the pH attained under the same conditions (c) plots of  $I_p$  of AM and AT vs. pH with error bars (d) plots of  $E_p$  of AM and AT vs. pH with their linear equations and error bars.

(Fig. S7†).<sup>34</sup> The slope values of  $E_p$  versus  $\log \nu$  show AM and AT oxidation are a two-electron process. Therefore, during the AM and AT oxidation process two electrons contribute to the electrochemical reaction at the nanosensor surface (Scheme 2).

**3.4.2. Effect of stripping electrolyte and pH.** The nature of stripping electrolytes and their pH values critically affect the analyte's interactions, redox reaction, and deposition process at the sensor surface. A series of the acidic, basic, neutral, and buffer stripping electrolytes as mentioned in Fig. 5a, were studied for AM and AT binary mixture at the COOH-CNTs/Ag/NH<sub>2</sub>-CNTs/GCE. The reproducible boosted oxidative signal values of AM and AT were observed in the PBS (pH 6). Therefore, it was chosen as the working medium for synchronized analysis of the drugs.

Thereafter, a variation of PBS pH values caused the current peak amplitude fluctuation, and a shift in peak potential suggests the involvement of protons during electrooxidation of the AM and AT at the electrode surface (Fig. 5b). The  $I_p$  of drugs increased gradually till pH 6 (Fig. 5c), which indicates that the AM ( $pK_a = 8.6$ ) and AT ( $pK_a = 4.5$ ) electroactive groups (involved in the oxidation process) exist in acid-base equilibrium.<sup>4,5</sup> At high pH, a decrease in  $I_p$  intensity associated with likely deprotonation of drugs and oxygen and nitrogen functionalities of the COOH-CNTs/Ag/NH<sub>2</sub>-CNTs nanocomposite, produce electrostatic repulsion at the sensor/electrolyte interfaces.

Thereby, the reduced voltammetric response at higher pH is ascribed to the kinetically poor feasibility of oxidation reactions due to unstable and inefficient adsorption of the analytes. Thus, to synchronously achieve an excellent sensitivity, boosted oxidation, and better resolution of AM-AT binary mixture at

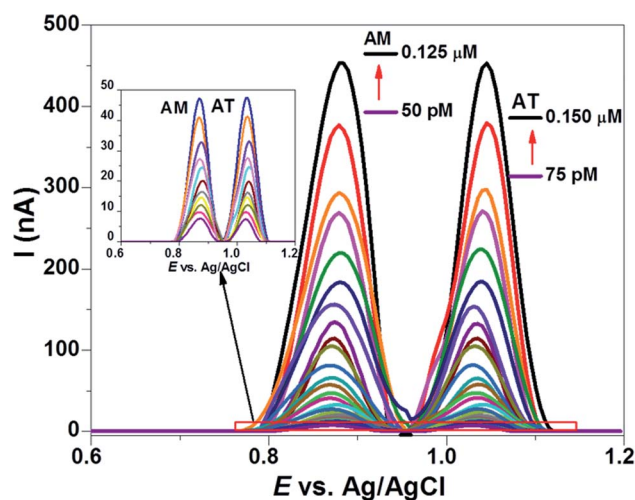


Fig. 6 SWASVs recorded by synchronized concentration variation of AM and AT in PBS of pH = 6 at 100  $mV s^{-1}$  scan rate, 0 V deposition potential, and 125 s accumulation time.



COOH-CNTs/Ag/NH<sub>2</sub>-CNTs/GCE, the PBS of pH 6 was employed in succeeding work. Furthermore, the linear plots of AM and AT peak potentials ( $E_p$ ) vs. pH (Fig. 5d) were almost parallel that signifies the fixed peak to peak potential difference in the studied pH range. Moreover, the slope values of 29 mV pH<sup>-1</sup> and 32 mV pH<sup>-1</sup> is closest to half of the Nernst value (59 mV pH<sup>-1</sup>) suggest two electrons and one proton are involved in the rate-determining steps of AM and AT electrooxidation at the modified electrode surface.<sup>4</sup>

### 3.5. Proposed oxidation mechanism of AM and AT

Based on the scan rate and pH variation results of CV and SWASV, an understanding of electroactive centers involved in the electrochemical oxidation reaction mechanisms of AM and AT drugs can be established. Chemical name of AM is 3-ethyl 5-methyl 2-[(2-aminoethoxy)methyl]-4-(2-chlorophenyl)-6-methyl-1,4-dihydropyridine-3,5-dicarboxylate.<sup>2</sup> A probable electrochemical reaction center of AM is its 1,4-dihydropyridine (1,4-DHP) unit which can oxidize in two steps anodic process. First, 1,4-DHP gets converted into cation at the interacting N-H bond through the removal of two electrons and one proton ( $2e^-/1H^+ \approx 1H^-$ ). Based upon the obtained experimental results overall oxidation of AM occurs by  $2e^-/2H^+$  process.

The AT is chemically (3*R*,5*R*)-7-[2-(4-fluorophenyl)-3-phenyl-4-(phenylcarbamoyl)-5-propan-2-ylpyrrol-1-yl]-3,5-dihydroxyheptanoic acid.<sup>6</sup> In CV and SWASV profiles, a single oxidation peak of AT is observed. Experimental results of the involvement of protons and electrons demonstrate a  $2e^-/1H^+$  oxidation process. The simplified proposed mechanistic pathway for the electrooxidation of AM and AT by transfer of  $2e^-/1H^+ \approx 1H^-$  can be seen in Scheme 2.<sup>1</sup>

### 3.6. Assessment of analytical features

The figures of merit (FOM) such as linearity ranges (LRs), limit of detection (LOD), the limit of quantification (LOQ), selectivity, specificity, repeatability, reproducibility, stability, storage capacity, reusability, precision, accuracy, % recovery, and practical applicability of the COOH-CNTs/Ag/NH<sub>2</sub>-CNTs/GCE were evaluated for AM-AT binary mixture by SWASV method under optimized conditions. The resultant analytical features

are statistically compiled in Table 2, signifying the applicability of our electroanalytical platform.

**3.6.1. The LCRs, LODs, and LOQs of the AM-AT.** The limit of detection (LOD) and quantification (LOQ) of the sensor can be assessed from their IUPAC standard definitions ( $LOD = 3\sigma/m$  and  $LOQ = 10\sigma/m$ ), where  $\sigma$  represents the standard deviation of  $n$  times replicate of voltammograms of sensor blank experiments (in electrolyte solution only) and  $m$  is the slope of calibration (concentration vs. current) plot. Likewise, the linear concentration ranges (LCRs) correspond to the minimum to the maximum concentrations range of analyte that follows a straight-line trend of the calibration plot. Thereby, the simultaneous quantitative assessment of AM and AT at the COOH-CNTs/Ag/NH<sub>2</sub>-CNTs/GCE, SWASV was carried out with AM-AT binary mixture in PBS pH 6 under optimized conditions. Fig. 6 shows stable and reproducible SW voltammograms of AM and AT with their synchronized concentration variation over the investigated range from 0.125  $\mu$ M to 50.0 pM and 0.50  $\mu$ M to 175.0 pM. Results show the steady rise in oxidation peak currents of AM and AT at 879 mV and 1040 mV with continuous addition of the drugs in the electrochemical cell. Likewise, the simultaneous analysis of AM and AT calibration plots signifies sensitivity and corresponding wide linear range of their oxidation peak currents and concentration. The voltammetric analysis of AM at the fabricated electrode exhibited LOD and LOQ, with values of 77.6 fM, and 258.6 fM, respectively. Likewise, the

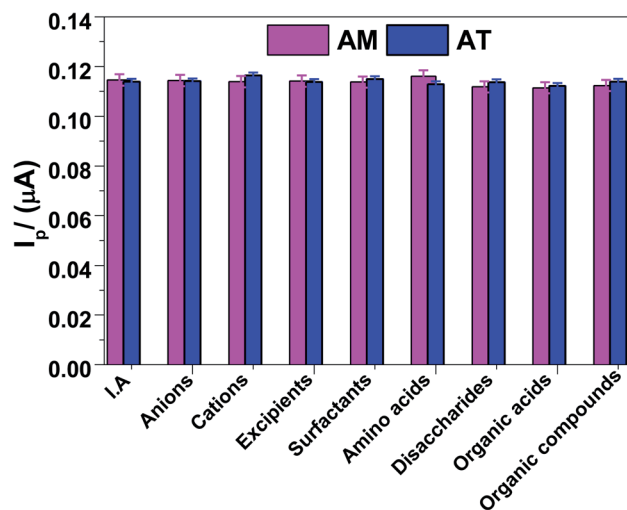


Fig. 7 Bar graphs with error bars obtained from the AM (6 nM) and AT (9 nM) voltammograms at COOH-CNTs/Ag/NH<sub>2</sub>-CNTs/GCE, in the co-existence of 2 mM of one of the organic and inorganic interferents, amino acids (alanine, cysteine, glutamic acid, glycine, lysine, leucine, threonine); cations (As<sup>3+</sup>, Ag<sup>+</sup>, Al<sup>3+</sup>, Ba<sup>2+</sup>, Cu<sup>2+</sup>, Cd<sup>2+</sup>, Cr<sup>3+</sup>, Ca<sup>2+</sup>, Cs<sup>+</sup>, Co<sup>2+</sup>, Fe<sup>3+</sup>, Hg<sup>2+</sup>, K<sup>+</sup>, Mn<sup>2+</sup>, Mg<sup>2+</sup>, Ni<sup>2+</sup>, NH<sub>4</sub><sup>+</sup>, Na<sup>+</sup>, Pb<sup>2+</sup>, Sr<sup>2+</sup>, Ti<sup>+</sup>, and Zn<sup>2+</sup>); anions (Cl<sup>-</sup>, CO<sub>3</sub><sup>2-</sup>, H<sub>2</sub>PO<sub>4</sub><sup>-</sup>, HCO<sub>3</sub><sup>-</sup>, NO<sub>3</sub><sup>-</sup>, and SO<sub>4</sub><sup>2-</sup>); organic acids (ascorbic acid, citric acid, folic acid, oxalic acid, succinic acid, salicylic acid, tannic acid, uric acid, usnic acid); disaccharides (fructose, glucose, galactose, lactose, maltose, sucrose); organic compounds (dopamine, EDTA, ethanol, glycerol, riboflavin, thymidine, urea, 2-amino-4-nitrophenol, 4-aminophenol, 3-chloro-5-nitrophenol), surfactants (CTAB, SDS); excipients (aerosol, magnesium stearate, TiO<sub>2</sub>, and starch), in PBS of pH = 6 under optimum SWASV conditions.

Table 2 Figures of merit of the COOH-CNTs/Ag/NH<sub>2</sub>-CNTs/GCE for the target drugs

Figures of merits	AM	AT
Investigated range ( $\mu$ M to pM)	0.125–50.0	0.15–75.0
Linearity range (nM to pM)	6–50	9–75
LOD (fM)	77.6 fM	83.2 fM
LOQ (fM)	258.6	277
% RSD (reproducibility) ( $n = 6$ )	<0.9	<0.9
% RSD (repeatability) ( $n = 5$ )	<1.5	<1.5
% RSD (stability) ( $n = 8$ )	1.5	2.7
% RSD (anti interference ability) ( $n = 20$ )	2.2	3.1
% RSD (validity) ( $n = 6$ )	<3	<3
% Recovery ( $n = 12$ )	95–102	96–103



LOD and LOQ of AT were found to be 83.2 fM, and 277 fM, respectively. These femtomole LODs are interrelated to the sensitivity and discrimination ability of the devised COOH-CNTs/Ag/NH<sub>2</sub>-CNTs/GCE for these coexisting exercised drugs even at minute concentrations.

### 3.6.2. Specificity, anti-interferent ability, and selectivity.

The major challenge in the detection of AM and AT drugs is the co-existing chemicals in physiological fluids and pharmaceutical dosage. To address this problem, a comparative electrochemical response of the target drugs was attained in presence of the interfering agents with their oxidation peaks obtained with standard solutions under optimized conditions. Hence, the influence of possible interferents such as amino acids, cations, anions, organic acids, disaccharides, surfactants, organic compounds, and excipients on oxidation peak currents of target analytes was probed by analyzing 6 nM AM, and 9 nM AT mixture (Fig. 7). The tolerable range was expressed as the maximum amount of the external agents that may cause <5%

relative error in the detection of target substrates. Thereby, the tolerance range of the sensor was noted as a % relative standard deviation (RSD) of <5% for these interferents with the sharp peaks of AM and AT without any distinctive peak of the interferents. These results manifest the excellent selectivity, anti-interferents activity, and specificity of the sensor and highlight its applicability in the assessment of real samples.

### 3.6.3. Reproducibility, reusability, and storage capability of the modified electrode.

The presented COOH-CNTs/Ag/NH<sub>2</sub>-CNTs electrochemical sensor was studied for accuracy and precision by analyzing its reproducibility and repeatability. The reproducibility was performed on the nanocomposite fabricated six different GCEs while the repeatability was evaluated over a regular time interval at the same electrodes, by SWASV of 6 nM AM and 9 nM AT in PBS (pH 6) (Fig. 8). The designed electrode presented a reproducible response from these six independent modified electrodes with the percent RSD of 0.9%, presenting reliability of the electrode for AM-AT detection

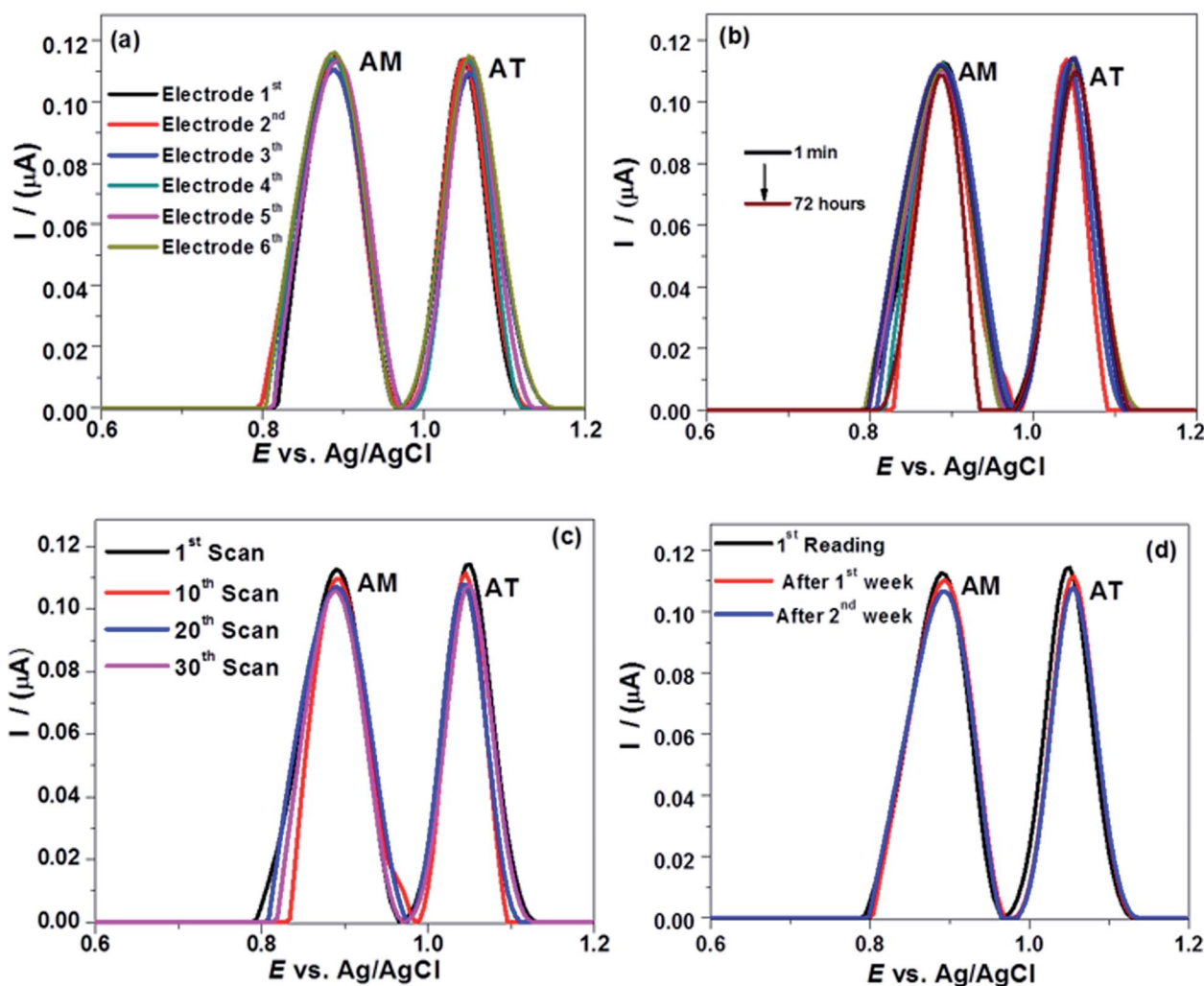


Fig. 8 Validity of the proposed procedure attested by inspecting the SWASV peak current  $I_p$  responses of AM (6 nM) and AT (9 nM) under established optimized settings (a) display reproducibility of the fabricated COOH-CNTs/Ag/NH<sub>2</sub>-CNTs/GCEs ( $n = 6$ ), (b) showing repeatability and stability of the COOH-CNTs/Ag/NH<sub>2</sub>-CNTs/GCE at intra and inter days scans ( $n = 8$ ), (c) presenting stability of the designed sensor ( $n = 10, 20, 30$ ), (d) illustrating long-term stability of the designed sensor.





(Fig. 8a). It also showed repeatability of 1.5% RSD after several intraday and inter-day repetitive analyses of similar fresh solutions (Fig. 8b). The COOH-CNTs/Ag/NH<sub>2</sub>-CNTs/GCE was kept in a vacuum desiccator at room temperature when not in use during repeatability and reusability analysis of the sensor. Moreover, the stability was investigated by applying the sensor for continuous SWASV scans against AM-AT, and after 10, 20, and 30 readings, the presented sensor has 98.1%, 96.2%, and 95.4% stability, respectively (Fig. 8c). Additionally, the long-term stability of the designed sensor for AM-AT was assessed by dipping it in PBS at room temperature for four weeks, and then analyzed by SWASV. The long-lasting stability was found to be 97.5% and 95.16% after two and four weeks, respectively from the initial current response (Fig. 8d). Conclusively, the repeatability, reproducibility, and long-term stability of the COOH-CNTs/Ag/NH<sub>2</sub>-CNTs/GCE were all tolerable (>95%) thereby, verify its good reliability and practicability for sensitive quantification of AM-AT in real matrixes.

**3.6.4. Percent recoveries in real sample at the designed electrode.** For adequacy and application of the recommended COOH-CNTs/Ag/NH<sub>2</sub>-CNTs/GCE based methodology, AM-AT were simultaneously assessed in multiple simple and complex real samples such as generic pharmaceutical dosage of AM, AT, AM-AT, serum, urine, tap & drinking water, artificial saliva, and synthetic sweat by the usual addition method. Firstly, in all samples, the initial amounts of AM-AT were analyzed by the SWASVs in their adequate dilutions without any prior excipient's separation. Then, the known quantities of the AM-AT from their standard solutions were spiked to the real samples, and % recoveries were estimated by the equivalent  $I_p$  values of AM-AT on established calibrations curves. The analysis was performed in three matrixes of each real sample and each voltammogram was triplicated. The initial amounts of AM and AT were attained analogous to the labeled claim of generic pharmacological formulations. However, no initial content of the AM-AT was

determined in all remaining real matrixes. Furthermore, % recoveries were obtained in the range of 97% to 103% with % RDS less than 3% as summarized in Table S1.† Henceforth, these results verify the effective reliability, specificity, and validity of the COOH-CNTs/Ag/NH<sub>2</sub>-CNTs/GCE for feasible clinical analysis.

**3.6.5. Comparative analysis with previously reported sensing platforms.** An evaluation of the analytical features of the presented COOH-CNTs/Ag/NH<sub>2</sub>-CNTs/GCE based analytical methodology, a comparison to the previously reported methods for the individual, and simultaneous detection of AM and AT was made and results are presented in Table 3. The SW stripping method apart from its requisite of surface modification of electrode and pre-concentration phases offer better assessment than other techniques.<sup>2,7,10</sup> Remarkably, the LODs values for the cited drugs accomplished by using our innovative sandwiched nanosensor are far lower than those attained by other sensors.<sup>2-7,10,14,15</sup> Hence, the devised electrochemical nanosensor provides superior sensitivities, linear ranges, lifetime and stability than many biomaterials, graphene-based electrodes, organic ligands, inorganic/organic polymers and their composites based on earlier reported sensors for AM and AT drugs.<sup>2-7,10,14,15</sup> Moreover, the CNTs-metallic sandwiched electrochemical nanosensor for the concurrent sensing of AM and AT has not been reported yet.

### 3.7. Theoretical studies of AM and AT at the designed electrode

The sensing process mainly consists of the drug molecules' adsorption, charge transduction, and the synergy among the layers of the nanocomposite.<sup>20</sup> To have insights on molecular level interactions, the potency of AM and AT with the nanocomposite sensor, theoretical factors were analyzed to correlate their qualitative propensities with experimental voltammetric analysis. The HOMO and LUMO of the AM and AT optimized

**Table 3** Assessment of the FOM of the designed COOH-CNTs/Ag/NH<sub>2</sub>-CNTs/GCE for the sensing of AM and AT with reported methods

Sensing platform	Measurement technique	LOD (nM)		Ref.
		AM	AT	
Acquity HSS C18	UPLC <sup>a</sup>	27	—	2
X Bridge® RP-18	HPLC	66	—	2
GCE	SWV	2.45	—	2
SPE	SWV	20.7	—	3
DNA/SPE	SWV	14.9	—	3
BDDE	DPV	70	—	4
MEKC	—	—	$3.3 \times 10^4$	5
PPY-GNs/GCE	DPV	—	1191	6
Spectro-fluorimetry	—	129.6	179	7
Waters C18	HPLC	2126	2057	7
I <sub>2</sub> /acetonitrile	UV-vis spectroscopy	—	100.3	10
GCE	DPV <sup>b</sup>	801	595	14
MWCNTs/GPE	DPV	4475	2446	15
COOH-CNTs/Ag NPs/NH <sub>2</sub> -CNTs/GCE	SWASV	77.6 fM	83.2 fM	This work

<sup>a</sup> UPLC = ultra-performance liquid chromatography; HPLC = high-performance liquid chromatography; SPE = screen printed electrode; DPV = differential pulse voltammetry; BDDE = boron-doped diamond electrodes; MEKC = micellar electrokinetic capillary chromatographic method; PPY-GNs = polypyrrole functionalized graphene sheets. <sup>b</sup> First derivative of ratio DPV technique.



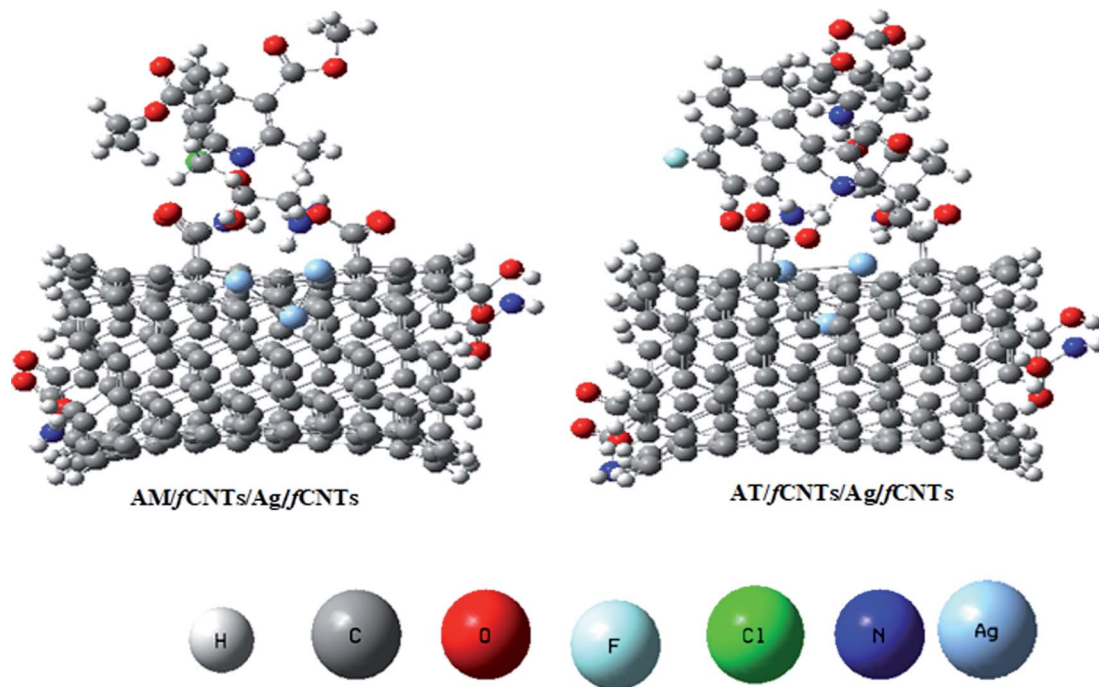


Fig. 9 The optimized structures of COOH-CNTs/Ag/NH<sub>2</sub>-CNTs merged systems with AM and AT by M06-2X method on Gaussian 09 software.

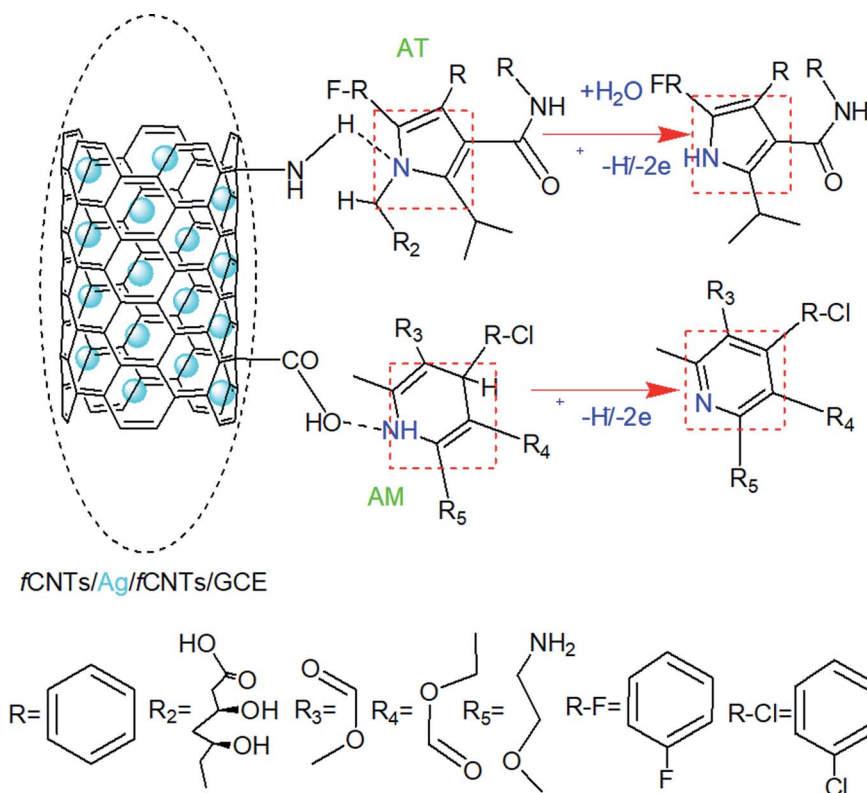
molecular geometries can be seen in Fig. S8†. Where, the negative binding energies ( $\Delta E$ ) of the AM (−24.5 eV), and AT (−13.6 eV) at Ag NPs specify the release of energies owing to the drugs' non-covalent interactions with Milliken charges of Ag NPs. The Ag NPs provide a high binding surface for the drug interactions to activate the N–H of 1,4 DHP unit of AM, and C–N–C of pyrrole units of AT, owing to its high electronegativity ( $\chi$ ). Likewise, the decrease of AM–AT band gap ( $E_g$ ) values correspond to an increase of chemical reactivity (oxidation ability) of the drugs and enhance charge transfer between their polarizable molecules and sensor surface.<sup>27</sup> Furthermore, the Ag/NH<sub>2</sub>-CNTs/drugs merged systems have  $\Delta E(\text{AM})$  −32.65 eV, and  $\Delta E(\text{AT})$  −19.1 eV, and decrease  $E_g$  values of AM–AT which verify their stable adsorption and ease of oxidation at lower overpotential values owing to more polarizable (softer) molecules (Fig. 3). Accordingly, the adsorption energies at NH<sub>2</sub>-CNTs/Ag/COOH-CNTs system, which was designated as the sensor surface for AM and AT electrochemical analysis, were  $\Delta E(\text{AM})$  −122 eV, and  $\Delta E(\text{AT})$  −98 eV which indicate enhanced analyte capturing ability of the multilayer nanocatalyst surface than the Ag NPs and Ag/COOH-CNTs surfaces (Fig. S9†). Likewise, the AM and AT electronic properties at the theoretical sensor surface support the experimental EIS, CV, and SWASV observations on the sequence of the fabricated electrodes sensing, NH<sub>2</sub>-CNTs/Ag/COOH-CNTs > Ag/COOH-CNTs > Ag NPs for the drugs electrooxidation at the lowest overpotential (Fig. 2 and 3, S8†). In addition, the AM–AT drugs  $\Delta E$ , quantum descriptors, and reactivities presented in Table S2† depict a trend of AM > AT at the NH<sub>2</sub>-CNTs/Ag/COOH-CNTs which is according to their experimental LODs calculated by SWASV (Section 3.6.1, Fig. 9). Lastly, all the theoretical analysis steps

collectively endorse the validity of the AM–AT binary mixture experimental oxidation results and the NH<sub>2</sub>-CNTs/Ag/COOH-CNTs nanocatalysts working mechanism.

#### 4. The COOH-CNTs/Ag NPs/NH<sub>2</sub>-CNTs/GCE sensing mechanism

The superior voltammetric performance of the electrochemical nanosensor is credited to the mutual correlation of intercalated Ag NPs with fCNTs matrix (Fig. 2 and 3). The *in situ* electroactive functionalities, porous texture, and conductive channels at the COOH-CNTs/Ag/NH<sub>2</sub>-CNTs nanocomposite facilitate the redox reactions by facilitating the transfer of electrons/protons effectively from AM and AT molecules to its surface in response to the applied potential. Thus, it works as a highly efficient biocompatible electrocatalyst to lower the AM–AT potentials, with a very high effective surface area provided by CNTs together with non-agglomerated Ag NPs (Fig. 1). For instance, the oxygen and nitrogen functionalities of the fCNTs act as anchoring sites to form hydrogen bonds which are responsible for their increased adsorption as suggested by the pH study (Section 3.4.2, Scheme 3).<sup>34</sup> In addition, the hydrogen bonds may also be formed between the chemisorbed analytes and their aqueous dissolved species. Likewise, the CNTs rings offer additional  $\pi$ – $\pi$  interactions to the AM and AT aromatic units *via* solute–sorber interactions during the preconcentration step of SWASVs. That in turn boosts the regional concentrations by selective adsorption of the analytes at CNTs with different resistance.<sup>34</sup> Moreover, the Ag NPs electrocatalytic activity for oxidation the cited drugs occurs at the Ag nuclei surface active sites and the mechanism is like a conventional heterogeneous





**Scheme 3** Oxidation mechanism of the AM and AT at the designed sensor COOH-CNTs/Ag/NH<sub>2</sub>-CNTs/GCE surface.

catalysis process.<sup>21,35</sup> Thereby, the electro-oxidation of AM to pyridine derivative and AT to 1*H*-pyrroly product *via* proton-coupled electron transfer ensued at NH<sub>2</sub>-CNTs/Ag/COOH-CNTs/GCE. Further, the anti-interference tests support this selective adsorption of target drugs at the designed medical nanosensor (Section 3.6.2). Likewise, the theoretical studies also evidence the existence of such favorable non-covalent host (drugs)-guest interactions at the interface (Section 3.7). However, the oxidation rate of the cited drugs affected by their electroactivities at the sensor surface owing to the number and strength of H-bonds,  $\pi$ - $\pi$  interactions, different charge distributions, and structural conformations. Conclusively, the overall oxidation of AM and AT based on electrocatalytic mechanisms of the NH<sub>2</sub>-CNTs/Ag/COOH-CNTs sandwiched matrix evidenced by foregoing EIS, CV, and SWASV results, is presented in Scheme 3.

## 5. Conclusion and future prospective

A highly sensitive and selective electrochemical sensing platform made of GCE modified with COOH-CNTs/Ag/NH<sub>2</sub>-CNTs nanocomposite was prepared for the analysis of the redox behavior of amlodipine (AM) and atorvastatin (AT). The as-prepared nanocomposite possessing Ag NPs embedded in fCNTs porous matrix demonstrated faster charge transduction for the redox probe. The mechanistic studies of the drugs at the designed electrode surface revealed the removal of 1H<sup>+</sup> in the oxidation processes of the respective drugs, where the host-

guest interaction of the cited drugs enabled the quantification of AM and AT up to femtomolar concentration. Regarding anti-interference test, the electrochemical sensing platform presented antifouling properties with specificity towards AM and AT in the presence of multi-fold higher concentration of foreign species. Moreover, the synergy among fCNTs and Ag NPs led to increased sensitivity for target analytes. High percentage recoveries of the selected drugs at the designed sensor validated practicability of the proposed methodology. Theoretical outcomes revealed interactions among the Ag NPs and fCNTs layers and with the drugs which resulted in stable adsorption of the AM-AT at the sensing surface. Hence, COOH-CNTs/Ag/NH<sub>2</sub>-CNTs hybrid nanocomposite-based electrode is expected to be a systematic benchmark for quality control laboratories to assess the drugs in medicinal and biological samples.

## Content presented in the ESI†

Experimental setup of electrochemical characterization and analysis (Fig. S1); UV-vis spectroscopy (Fig. S2); optimization of SWASV experimental parameters; SWASV response dependent on modifier type (Table S1); performance tests of sensors developed by different methods (Fig. S3); SWASV response dependent on modifier amount (Fig. S4); the influence of pre-concentration steps, accumulation potential on the current response of AM and AT (Fig. S5); deposition time on the AM and AT peaks intensities (Fig. S6); plot of AM and AT *I*<sub>p</sub> vs. log(scan rate) with error bar and respective linear equation (Fig. S7); real



sample analyses and standard addition recovery studies (Table S2); pictorial representation of HOMO and LUMO of optimized structures of AM and AT along with their energy gaps by DFT on Gaussian 09 software B3YLP method with basis set 6-311G++(d, p) (Fig. S8); the optimized structures of Ag NPs (triangle), COOH-CNTs (armchair (5, 5) with four COOH groups), NH<sub>2</sub>-CNTs (armchair (5, 5) with four CONH<sub>2</sub> groups) and their Ag /COOH-CNTs, and COOH-CNTs/Ag/NH<sub>2</sub>-CNTs merged systems with AM and AT by M06-2X method on Gaussian 09 software (Fig. S9); comparative data of the AM and AT with their Ag NPs, Ag NPs/COOH-fCNTs and NH<sub>2</sub>-CNTs/Ag NPs/COOH-CNTs merged systems and quantum descriptors (in terms of Hartree units) calculated by M06-2X method (Table S3).

## Conflicts of interest

There are no conflicts to declare.

## Acknowledgements

Dr Afzal Shah acknowledges the support of Quaid-i-Azam University and Higher Education Commission of Pakistan for supporting this work.

## References

- 1 I. Antal, M. Koneracka, V. Zavisova, M. Kubovcikova, Z. Kormosh and P. Kopcansky, Statins determination: a review of electrochemical techniques, *Crit. Rev. Anal. Chem.*, 2017, **47**, 474–489.
- 2 N. Karadas-Bakirhan, M. Gumustas, B. Uslu and S. A. Ozkan, Simultaneous determination of amlodipine besylate and rosuvastatin calcium in binary mixtures by voltammetric and chromatographic techniques, *Ionics*, 2016, **22**, 277–288.
- 3 M. Khairy, A. A. Khorshed, F. A. Rashwan, G. A. Salah, H. M. Abdel-Wadood and C. E. Banks, Sensitive determination of amlodipine besylate using bare/unmodified and DNA-modified screen-printed electrodes in tablets and biological fluids, *Sens. Actuators, B*, 2017, **239**, 768–775.
- 4 L. Švorc, K. Cinková, J. Sochr, M. Vojs, P. Michniak and M. Marton, Sensitive electrochemical determination of amlodipine in pharmaceutical tablets and human urine using a boron-doped diamond electrode, *J. Electroanal. Chem.*, 2014, **728**, 86–93.
- 5 B. Nigović, M. Damić, R. Injac, N. K. Glavač and B. Štrukelj, Analysis of atorvastatin and related substances by MEKC, *Chromatographia*, 2009, **69**, 1299–1305.
- 6 L. Wei, H. Yang, J. Jiao and B. Roth, Electrochemical sensor for ultrasensitive determination of atorvastatin based on polypyrrole functionalized graphene sheets, *Int. J. Electrochem. Sci.*, 2018, **13**, 10173–10180.
- 7 B. A. Moussa, A. A. El-Zaher, M. A. Mahrouse and M. S. Ahmed, Simultaneous determination of amlodipine besylate and atorvastatin calcium in binary mixture by spectrofluorimetry and HPLC coupled with fluorescence detection, *Anal. Chem. Insights*, 2013, **8**, 12921–12927.
- 8 N. Jadon, R. Jain, S. Sharma and K. Singh, Recent trends in electrochemical sensors for multianalyte detection: a review, *Talanta*, 2016, **161**, 894–916.
- 9 P. A. Chawla and S. Pandey, Various analytical methods for analysis of atorvastatin: a review, *J. Drug Delivery Ther.*, 2019, **9**, 885–899.
- 10 A. A. Ramadan, H. Mandil and J. Sabouni, Determination of atorvastatin calcium in pure and its pharmaceutical formulations using iodine in acetonitrile by UV-Visible spectrophotometric method, *Int. J. Pharm.*, 2015, **7**, 427–433.
- 11 Y. Kadioglu and M. Ozturk, Spectrofluorimetric determination of amlodipine in human plasma without derivatization, *Braz. J. Pharm. Sci.*, 2012, **48**, 719–725.
- 12 G. Ozcelikay, L. Karadurmus, S. I. Kaya, N. K. Bakirhan and S. A. Ozkan, A review: new trends in electrode systems for sensitive drug and biomolecule analysis, *Crit. Rev. Anal. Chem.*, 2020, **50**, 212–225.
- 13 S. A. Ozkan, J. M. Kauffmann and P. Zuman, *Electroanalysis in biomedical and pharmaceutical sciences*, Springer, 2019, vol. 3, pp. 11–26.
- 14 B. Dogan-Topal, B. Bozal, B. T. Demircigil, B. Uslu and S. A. Ozkan, Electroanalytical studies and simultaneous determination of amlodipine besylate and atorvastatin calcium in binary mixtures using first derivative of the ratio-voltammetric methods, *Electroanalysis*, 2009, **21**, 2427–2439.
- 15 A. Mohammadi, A. B. Moghaddam, K. Eilkanizadeh, E. Alikhani, S. Mozaffari and T. Yavari, Electro-oxidation and simultaneous determination of amlodipine and atorvastatin in commercial tablets using carbon nanotube modified electrode, *Micro Nano Lett.*, 2013, **8**, 413–417.
- 16 S. A. Ozkan, Principles and techniques of electroanalytical stripping methods for pharmaceutically active compounds in dosage forms and biological samples, *Curr. Pharm. Anal.*, 2009, **5**, 127–143.
- 17 B. Uslu and S. A. Ozkan, Electroanalytical application of carbon based electrodes to the pharmaceuticals, *Anal. Lett.*, 2007, **40**, 817–853.
- 18 S. Kurbanoglu and S. A. Ozkan, Electrochemical carbon based nanosensors: A promising tool in pharmaceutical and biomedical analysis, *J. Pharm. Biomed. Anal.*, 2018, **147**, 439–457.
- 19 T. Kokab, A. Munir, A. Shah, S. Kurbanoglu, M. A. Zia and S. A. Ozkan, *The effect of nanomaterials on the drug analysis performance of nanosensors, in new developments in nanosensors for pharmaceutical analysis*, Elsevier, 1st edn, 2019, pp. 79–118.
- 20 W. Yang, P. Thordarson, J. J. Gooding, S. P. Ringer and F. Braet, Carbon nanotubes for biological and biomedical applications, *Nanotech*, 2007, **18**(41), 412001.
- 21 N. K. Bakirhan, A. Shah and S. A. Ozkan, *Noble metal nanoparticles in electrochemical analysis of drugs in new developments in nanosensors for pharmaceutical analysis*, Elsevier, 1st edn, 2019, pp. 171–195.
- 22 S. W. Lee, B. S. Kim, S. Chen, Y. Shao-Horn and P. T. Hammond, Layer-by-layer assembly of all carbon





- nanotube ultrathin films for electrochemical applications, *J. Am. Chem. Soc.*, 2009, **131**, 671–679.
- 23 J. Xu, Y. Yokota, R. A. Wong, Y. Kim and Y. Einaga, Unusual electrochemical properties of low-doped boron-doped diamond electrodes containing  $\text{sp}^2$  carbon, *J. Am. Chem. Soc.*, 2020, **142**, 2310–2316.
- 24 V. Schroeder, S. Savagatrup, M. He, S. Lin and T. M. Swager, Carbon nanotube chemical sensors, *Chem. Rev.*, 2018, **119**, 599–663.
- 25 A. M. Campos, P. A. Raymundo-Pereira, C. D. Mendonça, M. L. Calegari, S. A. Machado and O. N. Oliveira Jr, Size control of carbon spherical shells for sensitive detection of paracetamol in sweat, saliva, and urine, *ACS Appl. Nano Mater.*, 2018, **1**, 654–661.
- 26 S. Esmailzadeh and G. Mashhadiagha, Formation constants and thermodynamic parameters of bivalent Co, Ni, Cu and Zn complexes with Schiff base ligand: Experimental and DFT calculations, *Bull. Chem. Soc. Ethiop.*, 2017, **31**, 159–170.
- 27 B. B. Dale, R. D. Senanayake and C. M. Aikens, Research Update: Density functional theory investigation of the interactions of silver nanoclusters with guanine, *APL Mater.*, 2017, **5**, 053102.
- 28 M. Sadaqat, L. Nisar, N. U. A. Babar, F. Hussain, M. N. Ashiq, A. Shah, M. F. Ehsan, M. Najam-Ul-Haq and K. S. Joya, Zinc-telluride nanospheres as an efficient water oxidation electrocatalyst displaying a low overpotential for oxygen evolution, *J. Mater. Chem. A*, 2019, **7**, 26410–26420.
- 29 B. Chen, Z. Zhu, J. Ma, Y. Qiu and J. Chen, Surfactant assisted Ce-Fe mixed oxide decorated multiwalled carbon nanotubes and their arsenic adsorption performance, *J. Mater. Chem. A*, 2013, **1**, 11355–11367.
- 30 R. Sharma, S. Tahiliani, N. Jain, R. Priyadarshi, S. Chhangani, S. Purohit and P. Joshi, Cynodon dactylon leaf extract assisted green synthesis of silver nanoparticles and their anti-microbial activity, *Adv. Sci., Eng. Med.*, 2013, **5**, 858–863.
- 31 J. Shen, W. Huang, L. Wu, Y. Hu and M. Ye, Study on amino-functionalized multiwalled carbon nanotubes, *Mater. Sci. Eng., A*, 2007, **464**, 151–156.
- 32 S. Wulandari, H. Widiyandari and A. Subagio, Synthesis and characterization carboxyl functionalized multi-walled carbon nanotubes (MWCNT-COOH) and  $\text{NH}_2$  functionalized multi-walled carbon nanotubes (MWCNT $\text{NH}_2$ ), *J. Phys.: Conf. Ser.*, 2018, **1025**, 012005–012011.
- 33 N. Li, Q. Li, X. R. Chen, A. J. Veloso, V. W. S. Hung, D. Dhar and K. Kerman, Au Nanoparticle-based detection of human chorionic gonadotropin using electrochemical impedance spectroscopy, *ECS Trans.*, 2013, **50**, 15–21.
- 34 A. U. Alam, Y. Qin, M. Catalano, L. Wang, M. J. Kim, M. M. Howlader, N.-X. Hu and M. J. Deen, Tailoring MWCNTs and  $\beta$ -cyclodextrin for sensitive detection of acetaminophen and estrogen, *ACS Appl. Mater. Interfaces*, 2018, **10**, 21411–21427.
- 35 Y. Zhao, Y. Yang, L. Cui, F. Zheng and Q. Song, Electroactive Au@Ag nanoparticles driven electrochemical sensor for endogenous  $\text{H}_2\text{S}$  detection, *Biosens. Bioelectron.*, 2018, **117**, 53–59.

